# A Mesozoic fossil lagerstätte from 250.8 million years ago shows a modern-type marine ecosystem.

Xu Dai, Joshua H.F.L. Davies, Zhiwei Yuan, Arnaud Brayard, Maria Ovtcharova, Guanghui Xu, Xiaokang Liu, Christopher P.A. Smith, Carrie E. Schweitzer, Mingtao Li, et al.

# A Mesozoic fossil lagerstätte from 250.8 Ma showing a modern-type marine ecosystem

**Authors:** Xu Dai[1, 2], Joshua H.F.L. Davies[3], Zhiwei Yuan[1], Arnaud Brayard[2], Maria Ovtcharova[4], Guanghui Xu[5, 6], Xiaokang Liu[1], Christopher P.A. Smith[2], Carrie E. Schweitzer[7], Mingtao Li[8], Morgann G. Perrot[3], Shouyi Jiang[1], Luyi Miao[1], Yiran Cao[1], Jia Yan[1], Ruoyu Bai[9], Fengyu Wang[1], Wei Guo[1], Huyue Song[1], Li Tian[1], Jacopo Dal Corso[1], Yuting Liu[1], Daoliang Chu[1], Haijun Song[1]*

**Affiliations:**

[1]State Key Laboratory of Biogeology and Environmental Geology, School of Earth Sciences, China University of Geosciences, Wuhan 430074, China

[2]Biogéosciences, UMR 6282, CNRS, Université de Bourgogne, 6 Boulevard Gabriel, 21000 Dijon, France

[3]Département des sciences de la Terre et de l'atmosphère, Université du Québec à Montréal/ GEOTOP, Montréal, H2X 3Y7, Canada

[4]Department of Earth Sciences, University of Geneva, rue des Maraîchers 13, Geneva, CH-1205, Switzerland

[5]Key Laboratory of Vertebrate Evolution and Human Origins of Chinese Academy of Sciences, Institute of Vertebrate Paleontology and Paleoanthropology, Chinese Academy of Sciences, Beijing, China

[6]CAS Center for Excellence in Life and Paleoenvironment, Beijing, China

[7]Department of Earth Sciences, Kent State University at Stark, North Canton, Ohio 44720, USA

[8]Institute of Geology and Paleontology, Linyi University, Linyi 276005, China

[9]Henan University of Engineering, Zhengzhou 451191, China

*Corresponding author, Email: haijunsong@cug.edu.cn

**Abstract:** Finely preserved fossil assemblages (lagerstätten) provide crucial insights into evolutionary innovations in deep time. We report an exceptionally preserved Early Triassic fossil assemblage, the Guiyang Biota, from the Daye Formation near Guiyang, South China. High-precision U-Pb dating shows that the age of the Guiyang Biota is 250.83 +0.07/-0.06 million years ago. This is only 1.08 ± 0.08 million years after the severe Permian-Triassic mass extinction, and this assemblage therefore represents the oldest known Mesozoic lagerstätte so far. The Guiyang Biota comprises at least 12 classes and 19 orders, including diverse fish fauna and malacostracans, revealing a trophically-complex marine ecosystem. The Guiyang Biota indicates rapid rise of modern-type marine ecosystems after the Permian-Triassic mass extinction.

**One-Sentence Summary:** The Guiyang Biota represent the oldest fossil assemblage known that shows rapid rise of a modern-type marine ecosystem after the Permian-Triassic mass extinction.

**Main Text:**

Phanerozoic marine organisms can be divided into three great evolutionary faunas: (i) “trilobite-dominated” Cambrian Evolutionary Fauna, (ii) “brachiopod-dominated” Paleozoic

Evolutionary Fauna, and (iii) "mollusc-dominated" Modern Evolutionary Fauna, which still thrives in present-day oceans (*1*). The rise to dominance of the Modern Evolutionary Fauna happened after the Permian-Triassic mass extinction (PTME), also known as the "Great Dying" around the Permian-Triassic boundary, ~251.9 million years ago (Ma) (*2*), which wiped out more than 80% of marine species (*3, 4*). The subsequent recovery was a significant period of evolutionary changes, during which not only did modern marine ecosystems emerge (*5*), but also the onset of the Triassic Revolution (*6*). However, owing to the relative scarcity of Early Triassic fossil records for many marine groups, and especially the lack of exceptionally-preserved fossil assemblages, the timing and processes of the rise of modern-type marine ecosystems remain poorly understood (*5*).

Following the PTME, Early Triassic marine fossil communities were thought to be depauperate, poorly diversified, and dominated by abundant and cosmopolitan disaster or opportunistic taxa (*7-11*). A slow, trophically stepwise recovery model, from bottom-level primary producers to topmost predators, has been proposed (*7*), but this pattern is highly debated (*12*). Full re-establishment of complex marine ecosystems was thought to have not occurred until, ~10 million years (Myr) after the PTME, being represented by the Luoping Biota (*13*). However, recent fossil finds, for instance, the Spathian Paris Biota (~3 Myr after the PTME) from the western USA (*5, 14*) and the Spathian Chaohu Biota (~4 Myr after the PTME) from South China (*15-19*), indicate that diverse and trophically-complex marine ecosystems occurred in the late Early Triassic. Despite these late Early Triassic biotas, a 3 Myr gap still exists after the PTME, with no such biotas. This gap could be the consequence of recurrent environmental stresses, including high sea surface temperature (*20-21*), episodes of oceanic acidification (*22*), and anoxic/euxinic events (*23-24*) mainly occurring during the Permian-Triassic transition, the late Dienerian and late Smithian. Alternatively, it can also result from preservation and sampling biases, which are often neglected in many previous works (*5, 9*).

Here, we report an exceptionally-preserved fossil assemblage, named Guiyang Biota, from Guizhou Province, South China. The Guiyang Biota is late Dienerian in age (~1 Myr after the PTME) and it is therefore the oldest known Mesozoic fossil lagerstätte. The Guiyang Biota represents a diverse and trophically complex marine ecosystem and partially fills the 3 Myr gap of complex marine faunas, indicating a rapid rise of modern-type marine ecosystems after the PTME, despite global sea-surface temperatures remaining high.

## Geological setting

Specimens of the Guiyang Biota were found in the middle unit of the Lower Triassic Daye Formation at six sections near Guiyang, Guizhou Province (Fig. 1B, C). All these sections were located on the northern margin of the Nanpanjiang Basin, which was located in the eastern Tethys, near the equator, during the Early Triassic (Fig. 1A). The three best-exposed sections were measured and sampled at a high resolution (Fig. S1). The middle unit of the Daye Formation is characterized by alternating finely-laminated black shales and thin- to medium-bedded limestones (Figs. S2–S3). Carbonate concretions are also common and usually rich in pyrite framboids. No bioturbation has been observed within this interval. Microfacies analyses show that the thin-bedded limestones are pelagic wackestones with occasional occurrences of small foraminifers and ostracods (Fig. S4). There is no major difference in facies among the studied sections. The middle unit of the Daye Formation is thus interpreted to have been deposited in a deep shelf region of the northern Nanpanjiang Basin where oxygen-depleted environments frequently occurred (*25*).

## Age of the Guiyang Biota

The age of the Guiyang Biota is constrained to the late Dienerian by three independent methods (Fig. 1D): (i) ammonoid and conodont biostratigraphy, (ii) carbon isotope chemostratigraphy (Table S1) and (iii) high-precision U-Pb dating (Table S2). The

assemblage of ammonoids *Radioceras* sp. and conodonts *Neospathodus cristagalli* and *Neospathodus dieneri* indicates a late Dienerian age (Fig. S5). The Early Triassic carbon isotope curve displays four negative (N1–N4) and three positive (P1–P3) excursions, which can be correlated globally (*26*). At Gujiao, carbon isotope curve with biostratigraphic calibration indicates that the Guiyang Biota corresponds to the N2 (Fig. 1D), again supporting a late Dienerian age. Finally, high precision CA-ID-TIMS zircon U-Pb ages from two ash beds at Gujiao provide absolute time constraints for the Guiyang Biota. Zircons from sample GJ-ASH-134, ~3 m below the fossil interval, yield an age of 250.92 ± 0.15 Ma (2σ). The second ash sample GJ-ASH-157 occurring within the fossil interval at Gujiao yields an age of 250.766 ± 0.084 Ma (2σ). An age-depth model using the ages from these ash beds indicates that the lower and upper age limits of the Guiyang Biota are 250.83 +0.07/-0.06 Ma and 250.72 +0.09/-0.21 Ma, respectively. Hence, the Guiyang Biota spans an interval of 0.11 +0.21/-0.06 Myr and is 1.08 ± 0.08 Myr after the PTME (Fig. S6).

**Taxonomic composition**

One million years after the PTME, the Guiyang Biota shows an unexpectedly diversified assemblage, including coelacanths, actinopterygians, decapods, Cyclida, ammonoids, bivalves, conodonts, foraminifers, ostracods, sponges, radiolarians, and coprolites (Figs. 2–3, S7-S10, and Table S3). Sampled specimens are usually compressed in 2D, except for some bony fishes and ammonoids from calcareous concretions retaining 3D structures. Fishes, decapods, Cyclida and coprolites are all preserved in calcium phosphate (Figs. S11–S15). Sponge spicules and radiolarians are silicified. Foraminifers are usually calcareous, but some of them are pyritized (Fig. 3P).

Osteichthyes are the main component of the biota with two main groups: Actinistia (Fig. 2A) and Actinopterygii (Fig. 2B–F). Two different coelacanth species have been found so far and are the largest macrofossils in the Guiyang Biota. All these specimens show an estimated

body length of more than 0.5 m, with the largest specimen reaching a body length of approximately 1 m. More than 10 species of at least six actinopterygian orders have been identified, including stem actinopterygians (Palaeonisciformes and Ptycholepiformes), chondrosteans (Acipenseriformes), stem neopterygians (Perleidiformes *(27)* and Polzbergiiformes), and holosteans (Parasemionotiformes). Additionally, Chondrichthyes, represented by a hybodontiform tooth, have also been found (Fig. 2G–H).

Arthropods are the most abundant group. They are represented by malacostracans (Decapoda), ostracods, and Cyclida, which is an enigmatic crustacean group with a scarce fossil record and uncertain phylogeny. Among the decapods, two shrimp taxa are recognized as *Anisaeger* sp. (Fig. 3J-K) and an undetermined Aegeridae (Figs. 3E-I, S8, S13), which extend the temporal range of this family by 1.5 Myr to the Dienerian (*28*). The Aegeridae are thought to be the basal group for most modern shrimps (*28*). Therefore, the fossils of the Guiyang Biota represent some of the oldest known shrimps. One specimen of an undetermined litogastrid lobster (Fig. 3L) was also found, predating the previously oldest report of this group by nearly 1.5 Myr (*28*). Overall, this decapod fauna is the oldest known among the Early Triassic fauna documented so far (*5, 28, 29*). In addition, one specimen of Cyclida has been found (Fig. 3M–N and Fig. S14), which shows a close morphological affinity to *Yunnanocyclus nodosus* reported from the Anisian Luoping Biota (*30*), but differs mainly by shorter thoracic segmentations. Notably, this specimen represents the third reported occurrence of Early Triassic Cyclida, the others being from the Induan of Madagascar and Olenekian of Germany (*31*).

At least two ammonoid taxa were found in the Guiyang biota, *Pseudosageceras* sp. and *Radioceras* sp. (Figs. 3A-B, S9). Four bivalve genera were also recognized, *Eumorphotis*, *Claraia*, *Promyalina*, and *Modiolus* (Figs. 3C-D, S9). Isolated sponge spicules are common in some beds in the fossiliferous interval (Figs. 3Q, S10). One radiolarian taxon was found, *Latentifistula* sp. (Fig. S10), a long-ranging genus from the Permian to the Triassic.

Foraminifers are also common (Figs. 3P, S10), with seven species recognized (Table S3), of which *Postcladella kalhori* is the most abundant. This foraminifer fauna appears as one of the richest known so far for the Dienerian (*32*). Three conodont species, *Neospathodus kristagalli*, *Neospathodus dieneri*, and *Novispathodus posterolongatus*, were found within the fossiliferous interval at Gujiao (Fig. S5).

**Trophic and ecological structure**

This new assemblage is trophically-complex, including various representative species ranging from primary consumers, such as foraminifers, to large predators, such as coelacanths. Based on the trophic pyramid model of a fossilized marine ecosystem (*7*), the Guiyang Biota contains representatives of all trophic levels and represents a complete trophic pyramid (Fig. 4C). Although fossils of primary producers, such as algae, have not been found in the Guiyang Biota, their presence may be inferred as they are at the base of trophic networks. Primary consumers found in the biota consist of at least seven species of foraminifers, one radiolarian genus, and one taxon of sponges. Bivalves, including at least four genera, represent meso-consumers. Ammonoids and decapods are likely to have been predatory. Predatory fishes, represented mainly by coelacanth, are at the apex of trophic network of the Guiyang Biota. Conodonts may have acted as predators or scavengers in marine ecosystems (*33*). Additionally, the occurrence of vertebrate coprolites, ranging from 1 to 3 cm in diameter (Fig. 3O), confirms a complex trophic network. According to the theoretical ecospace model (*34*), which is based on six tiering positions, six motility levels and six feeding strategies for marine organisms, the Guiyang Biota includes at least ten ecological modes (Fig. S16), similar to those of younger renowned Triassic biotas (Fig. 4A, Tables S4, S5).

**Discussion**

The Guiyang Biota contains a diverse and trophically complex marine ecosystem and extends the occurrence of complex marine ecosystems to approximately one Myr after the PTME (Fig. 4B, C), representing oldest Mesozoic lagerstätte known to date. The Guiyang Biota shows that some significant groups of modern marine ecosystems, such as decapod arthropods and actinopterygian fishes experienced a more rapid post-PTME diversification than previously thought (*15, 28, 35*). Preservation and sampling biases have distorted our current understanding of the post-PTME recovery, and this report of a complex biota from ever closer to this event forces us to rethink interpretations of the biotic recovery after the PTME. The Guiyang Biota suggests that higher trophic levels were not completely eliminated by the PTME, or recovered rapidly driven by biotic interaction, such as interspecific competition *(36)*.

The Early Triassic is often portrayed as a super-greenhouse world (*20, 21*), in which life was expelled from the tropics leading to a poleward shift of tetrapods and a near absence of fish faunas within the tropics (*20, 37, 38*). Based on the new data from the Guiyang Biota, in the middle unit of the Daye Formation, the supposed tropical fish gap appears to be solely a product of sampling bias. The presence of fishes in the late Dienerian Guiyang Biota and in the late Smithian of South China (*39*) and the western USA basin (*40*) filled the tropical fish gap at least during these two periods of relative cooling *(20, 21)*. Thus, this suggests that the supposed tropical lethally hot temperature was not consistent throughout the whole Early Triassic, and likely fluctuated with some cooler periods corresponding to the thermal tolerances of marine fishes.

Although the Guiyang Biota remains incompletely sampled, it highlights that the slow and stepwise recovery model after the PTME is not applicable. The Guiyang Biota already fills part of a wide knowledge gap regarding the rise of modern marine ecosystems after the PTME by documenting the early diversification of fishes and decapods, two groups playing

significant role in present-day marine ecosystems and in prey-predator interactions during the Mesozoic Marine Revolution (*6*, *41*).

**References and Notes**


1. J. J. Sepkoski, A factor analytic description of the Phanerozoic marine fossil record. *Paleobiology* **7**, 36–53 (1981). DOI:10.1017/S0094837300003778
2. S. D. Burgess, S. Bowring, S.-Z. Shen, High-precision timeline for Earth's most severe extinction. *Proc. Natl. Acad. Sci. U.S.A.* **111**, 3316–3321 (2014). DOI:10.1073/pnas.1317692111
3. D. M. Raup, Size of the permo-triassic bottleneck and its evolutionary implications. *Science* **206**, 217–218 (1979). DOI:10.1126/science.206.4415.217
4. S. M. Stanley, Estimates of the magnitudes of major marine mass extinctions in earth history. *Proc. Natl. Acad. Sci. U.S.A.* **113**, E6325–E6334 (2016). DOI:10.1073/pnas.1613094113
5. A. Brayard *et al.*, Unexpected Early Triassic marine ecosystem and the rise of the Modern evolutionary fauna. *Sci. Adv.* **3**, e1602159 (2017). DOI:10.1126/sciadv.1602159
6. M. J. Benton, F. Wu, Triassic Revolution. *Front. Earth Sci.* **10**, 899541 (2022). DOI:10.3389/feart.2022.899541
7. Z.-Q. Chen, M. J. Benton, The timing and pattern of biotic recovery following the end-Permian mass extinction. *Nat. Geosci.* **5**, 375–383 (2012). DOI:10.1038/ngeo1475
8. D. J. Bottjer, M. E. Clapham, M. L. Fraiser, C. M. Powers, Understanding mechanisms for the end-Permian mass extinction and the protracted Early Triassic aftermath and recovery. *GSA Today* **18**, 4–10 (2008). DOI:10.1130/GSATG8A.1
9. A. Hallam, Why was there a delayed radiation after the end-Palaeozoic extinctions? *Hist. Biol.* **5**, 257–262 (1991). DOI:10.1080/1029238910938045

10. W. J. Foster, S. Danise, G. D. Price, R. J. Twitchett, Subsequent biotic crises delayed marine recovery following the late Permian mass extinction event in northern Italy. *PloS one* **12**, e0172321 (2017). DOI:10.1371/journal.pone.0172321

11. E. Petsios, D. J. Bottjer, Quantitative analysis of the ecological dominance of benthic disaster taxa in the aftermath of the end-Permian mass extinction. *Paleobiology* **42**, 380–393 (2016). DOI:10.1017/pab.2015.47

12. T. M. Scheyer, C. Romano, J. Jenks, H. Bucher, Early Triassic marine biotic recovery: the predators' perspective. *PloS one* **9**, e88987 (2014). DOI:10.1371/journal.pone.0088987

13. S. Hu *et al.*, The Luoping biota: exceptional preservation, and new evidence on the Triassic recovery from end-Permian mass extinction. *Proc. Royal Soc. B* **278**, 2274–2282 (2011). DOI:10.1098/rspb.2010.2235

14. C. P. A. Smith *et al.*, Exceptional fossil assemblages confrm the existence of complex Early Triassic ecosystems during the early Spathian. *Sci. Rep.* **11**, 19657 (2021). DOI:10.1038/s41598-021-99056-8

15. M. J. Benton *et al.*, Exceptional vertebrate biotas from the Triassic of China, and the expansion of marine ecosystems after the Permo-Triassic mass extinction. *Earth-Sci. Rev.* **125**, 199–243 (2013). DOI:10.1016/j.earscirev.2013.05.014

16. C. Ji, A. Tintori, D. Jiang, R. Motani, F. Confortini, New Thylacocephala (Crustacea) assemblage from the Spathian (Lower Triassic) of Majiashan (Chaohu, Anhui Province, South China). *J. Paleontol.* **95**, 305–319 (2020). DOI:10.1017/jpa.2020.92

17. D.-Y. Jiang *et al.*, A large aberrant stem ichthyosauriform indicating early rise and demise of ichthyosauromorphs in the wake of the end-Permian extinction. *Sci. Rep.* **6**, 26232 (2016). DOI:10.1038/srep26232.

18. R. Motani *et al.*, A basal ichthyosauriform with a short snout from the Lower Triassic of China. *Nature* **527**, 544–544 (2015). DOI:10.1038/nature13866

19. A. Tintori *et al.*, A new *Saurichthys* (Actinopterygii) from the Spathian (Early Triassic) of Chaohu (Anhui Province, China). *Riv. Ital. di Paleontol. e Stratigr.* **120**, 157–164 (2014). DOI:10.13130/2039-4942/6057

20. Y. Sun *et al.*, Lethally hot temperatures during the Early Triassic greenhouse. *Science* **338**, 366–370 (2012). DOI:10.1126/science.1224126

21. C. Romano *et al.*, Climatic and biotic upheavals following the end-Permian mass extinction. *Nat. Geosci.* **6**, 57–60 (2013). DOI:10.1038/ngeo1667

22. H. Song *et al.*, Conodont calcium isotopic evidence for multiple shelf acidification events during the Early Triassic. *Chem. Geol.* **562**, 120038 (2021). DOI:10.1016/j.chemgeo.2020.120038

23. P. B. Wignall, R. J. Twitchett, Oceanic anoxia and the end Permian mass extinction. *Science* **272**, 1155–1158 (1996). DOI:10.1126/science.272.5265.1155

24. S. E. Grasby, B. Beauchamp, A. Embry, H. Sanei, Recurrent Early Triassic ocean anoxia. *Geology* **41**, 175–178 (2013). DOI:10.1130/G33599.1

25. L. Tian *et al.*, Reconstruction of Early Triassic ocean redox conditions based on framboidal pyrite from the Nanpanjiang Basin, South China. *Palaeogeogr., Palaeoclimatol., Palaeoecol.* **412**, 68–79 (2014). DOI:10.1016/j.palaeo.2014.07.018

26. H. Song *et al.*, Large vertical $\delta^{13}C$ DIC gradients in Early Triassic seas of the South China craton: implications for oceanographic changes related to Siberian Traps volcanism. *Global Planet. Change* **105**, 7–20 (2013). DOI:10.1016/j.gloplacha.2012.10.023

27. Z. Yuan *et al.*, A new perleidid neopterygian fish from the Early Triassic (Dienerian, Induan) of South China, with a reassessment of the relationships of Perleidiformes. *PeerJ*, **10**, e13448 (2022). DOI: 10.7717/peerj.13448

28. C. P. A. Smith *et al.*, The Paris Biota decapod (Arthropoda) fauna and the diversity of Triassic decapods. *J. Paleontol.* 96, 1235–1263 (2022). DOI:10.1017/jpa.2022.34.

29. A. Garassino, G. Pasini, G. Teruzzi, Macrurans (Crustacea, Decapoda) from the Lower Triassic (Olenekian) of the Ambilobé area (NW Madagascar). *Contrib. to Zool.* **72**, 137–139 (2003). DOI:10.1163/18759866-0720203014

30. R. M. Feldmann *et al.*, A new Middle Triassic (Anisian) cyclidan crustacean from the Luoping Biota, Yunnan Province, China: morphologic and phylogenetic insights. *J. Crust. Biol.* **37**, 406–412 (2017). DOI:10.1093/jcbiol/rux052

31. C. E. Schweitzer, E. V. Mychko, R. M. Feldmann, Revision of Cyclida (Pancrustacea, Multicrustacea), with five new genera. *Neues Jahrb. Geol. Paläontol.* **296**, 1–59 (2020). DOI:10.1127/njgpa/2020/0905.

32. H. Song *et al.*, Recovery tempo and pattern of marine ecosystems after the end-Permian mass extinction. *Geology* **39**, 739–742 (2011). DOI:10.1130/G32191.1

33. M. A. Purnell, Microwear on conodont elements and macrophagy in the first vertebrates. *Nature* **374**, 798–800 (1995). DOI:10.1038/374798a0

34. R. K. Bambach, A. M. Bush, D. H. Erwin, Autecology amd the filling of ecospace: key metazoan radiations. *Palaeontology* **50**, 1–22 (2007). DOI:10.1111/j.1475-4983.2006.00611.x

35. C. Romano *et al.*, Permian–Triassic Osteichthyes (bony fshes): diversity dynamics and body size evolution. *Biol. Rev.* **91**, 106–147 (2016). DOI:10.1111/brv.12161

36. M. Hautmann *et al*., Competition in slow motion: the unusual case of benthic marine communities in the wake of the end‐Permian mass extinction. *Palaeontology*, **58**, 871–901 (2015). DOI: 10.1111/pala.12186

37. B. J. Allen, P. B. Wignall, D. J. Hill, E. E. Saupe, A. M. Dunhill, The latitudinal diversity gradient of tetrapods across the Permo-Triassic mass extinction and recovery interval. *Proc. Royal Soc. B* **287**, 20201125 (2020). DOI:10.1098/rspb.2020.1125

38. M. Bernardi, F. M. Petti, M. J. Benton, Tetrapod distribution and temperature rise during the Permian–Triassic mass extinction. *Proc. Royal Soc. B* **285**, 20172331 (2018). DOI:10.1098/rspb.2017.2331

39. J. Tong, X. Zhou, D. H. Erwin, J. Zuo, L. Zhao, Fossil fishes from the Lower Triassic of Majiashan, Chaohu, Anhui Province, China. *J. Paleontol.* **80**, 146–161 (2006). DIO:10.1666/0022-3360(2006)080[0146:FFFTLT]2.0.CO;2

40. C. Romano *et al.*, Marine Early Triassic Actinopterygii from Elko County (Nevada, USA): implications for the Smithian equatorial vertebrate eclipse. *J. Paleontol.* **91**, 1025–1046 (2017). DOI:10.1017/jpa.2017.36

41. G. J. Vermeij, Escalation and its role in Jurassic biotic history. *Palaeogeogr., Palaeoclimatol., Palaeoecol.* **263**, 3–8 (2008). DOI:10.1016/j.palaeo.2008.01.023

42. C. R. Scotese, Atlas of Middle & Late Permian and Triassic Paleogeographic maps, maps 43–48 from volume 3 of the PALEOMAP Atlas for ArcGIS (Jurassic and Triassic) and maps 49–52 from volume 4 of the PALEOMAP PaleoAtlas for ArcGIS (Late Paleozoic). *Mollweide Projection, PALEOMAP Project, Evanston, IL*, (2014). DOI:10.13140/2.1.2609.9209

43. X. Dai, H. Song, A. Brayard, D. Ware, A new Griesbachian–Dienerian (Induan, Early Triassic) ammonoid fauna from Gujiao, South China. *J. Paleontol.* **93**, 48–71 (2019). DOI:10.1017/jpa.2018.46

44. A. D. Muscente *et al.*, Exceptionally preserved fossil assemblages through geologic time and space. *Gondwana Res.* **48**, 164–188 (2017). DOI:10.1016/j.gr.2017.04.020

45. X. Dai *et al.*, R-scripts-Dai-et-al-2022. Zenodo (2022). DOI:10.5281/zenodo.7466123

46. Zhang, K. et al. Early Triassic conodont–palynological biostratigraphy of the Meishan D Section in Changxing, Zhejiang Province, South China. *Palaeogeogr. Palaeoclimatol. Palaeoecol.* **252**, 4–23, (2007). DOI:10.1016/j.palaeo.2006.11.031

47. Yan, C. et al. Uppermost Permian to Lower Triassic conodonts at Bianyang section, Guizhou Province, South China. *Palaios* **28**, 509–522, (2013). DOI:10.2110/palo.2012.p12-077r

48. Orchard, M. J. & Tozer, E. T. Triassic conodont biochronology, its calibration with the ammonoid standard, and a biostratigraphic summary for the Western Canada Sedimentary Basin. *Bull. Can. Pet. Geol.* **45**, 675–692, (1997). DOI:10.35767/gscpgbull.45.4.675

49. Lyu, Z., Orchard, M. J., Chen, Z.-Q., Henderson, C. M. & Zhao, L. A proposed ontogenesis and evolutionary lineage of conodont *Eurygnathodus costatus* and its role in defining the base of the Olenekian (Lower Triassic). *Palaeogeogr. Palaeoclimatol. Palaeoecol.* **559**, 109916, (2020). DOI:10.1016/j.palaeo.2020.109916

50. Ware, D., Bucher, H., Brayard, A., Schneebeli-Hermann, E. & Brühwiler, T. High-resolution biochronology and diversity dynamics of the Early Triassic ammonoid recovery: the Dienerian faunas of the Northern Indian Margin. *Palaeogeogr. Palaeoclimatol. Palaeoecol.* **440**, 363–373, (2015). DOI:10.1016/j.palaeo.2015.09.013

51. Widmann P., Davies, J.H.F.L & Schaltegger, U. Calibrating chemical abrasion: Its effects on zircon crystal structure, chemical composition and U-Pb age. *Chem Geol.* **511**, 1–10, (2019). DOI: 10.1016/j.chemgeo.2019.02.026

52. Condon, D. J., Schoene, B., McLean, N. M., Bowring, S. A. & Parrish, R. R. Metrology and traceability of U–Pb isotope dilution geochronology (EARTHTIME Tracer Calibration Part I). *Geochim. Cosmochim. Acta* **164**, 464–480, (2015). DOI:10.1016/j.gca.2015.05.026

53. McLean, N. M., Condon, D. J., Schoene, B. & Bowring, S. A. Evaluating uncertainties in the calibration of isotopic reference materials and multi-element isotopic tracers (EARTHTIME Tracer Calibration Part II). *Geochim. Cosmochim. Acta* **164**, 481–501, (2015). DOI:10.1016/j.gca.2015.02.040

54. Schaltegger, U. et al. Long-term repeatability and interlaboratory reproducibility of high-precision ID-TIMS U–Pb geochronology. *J. Anal. At. Spectrom.* **36**, 1466–1477, (2021). DOI:10.1039/D1JA00116G

55. McLean, N. M., Bowring, J. F. & Bowring, S. A. An algorithm for U-Pb isotope dilution data reduction and uncertainty propagation. *Geochem. Geophys. Geosyst.* **12**, Q0AA18, (2011). DOI:10.1029/2010GC003479

56. Parnell, A. C., Haslett, J., Allen, J. R., Buck, C. E. & Huntley, B. A flexible approach to assessing synchroneity of past events using Bayesian reconstructions of sedimentation history. *Quat. Sci. Rev.* **27**, 1872–1885, (2008). DOI:10.1016/j.quascirev.2008.07.009

57. T. Galfetti *et al*., Timing of the Early Triassic carbon cycle perturbations inferred from new U–Pb ages and ammonoid biochronozones. *Earth & Planet. Sci. Let.* **258**, 593–604, (2007). DOI:10.1016/j.epsl.2007.04.023

58. P. Widmann *et al*., Dynamics of the largest carbon isotope excursion during the Early Triassic biotic recovery. *Front. Earth Sci.* **8**, 196. DOI:10.3389/feart.2020.00196

**Acknowledgments:** We thank Wenwei Guo and Ying Ma for assistance in zircon analyses, Yi Wang for assistance in the field, and Dayou Zhai and Qianwei Wang for their help in taking fluorescence photographs at Yunnan University.

**Funding:**

National Natural Science Foundation of China (92155201, 41821001)

Strategic Priority Research Program of Chinese Academy of Sciences (XDB26000000)

111 Project (B08030)

Fundamental Research Funds for National University, China University of Geosciences (Wuhan)

China Scholarship Council (202006410051)

Programme TelluS of the INSU, CNRS (to AB)

French “Investissements d’Avenir” program (project ISITE-BFC: ANR-15-IDEX-03; to AB)

BQR of the Université de Bourgogne (to XD and AB)

**Author contributions:**

Conceptualization: XD, Haijun S

Field work: XD, XL, LM, YC, SJ, DC, ZY, Haijun S

Taxonomy: XD, ZY, XL, AB, GX, CPAS, CES, JY, RB, YL

Zircon analyses: JHFLD, MO, MGP, XD

XRF analyses: WG

SEM-EDS analyses: XD

Carbon isotope analyses: Huyue S

Writing – original draft: XD, Haijun S, AB

Writing – review & editing: all authors.

**Competing interests:** Authors declare that they have no competing interests.

**Data and materials availability:** All data are available in the main text or the supplementary materials. Data and code for rarefaction analysis are available at (*45*). All figured specimens are housed at the Yifu Museum of China University of Geosciences

(CUGM) and can be accessed by contacting the curator Jing Chen at the museum (jingchen@cug.edu.cn).

**Supplementary Materials**

Materials and Methods

Figs. S1 to S16

Tables S1 to S6

Data S1

## Figure legends

**Fig. 1. Geological context of the Guiyang Biota. (A–C)** Early Triassic and present-day locations of the studied exposures. Early Triassic paleogeographic map was modified from Scotese (*42*). **(D)** Synthetic regional lithological succession with associated carbon isotopic trend (analyzed in this study) and simplified estimated sea surface temperature (SST) modified from Sun et al. (*20*). Gr: Griesbachian, CX: Changxing Formation, DL: Dalong Formation. The yellow band indicates the stratigraphic position of the Guiyang Biota. Ammonoid zonation after Dai et al. (*43*): 1, *Ophiceras medium* beds; 2, *Jieshaniceras guizhouense* beds; 3, *Ambites radiatus* bed; 4, *Radioceras* sp. beds. Conodont zones: 5, *Neospathodus dieneri* Zone; 6, *Neospathodus cristagalli* Zone; 7, *Novispathodus waageni* Zone. The definitions of N2 and P2 of the carbon isotope curve refer to Song et al. (*26*).

**Fig. 2. Osteichthyes and Chondrichthyes from the Guiyang Biota. (A)** Coelacanthiformes indet. A, CUGM 00343, Gujiao. **(B)** Parasemionotiformes *Watsonulus* sp., CUGM 00344, Gaopo. **(C)** Polzbergiformes indet., CUGM 00345, Gujiao. **(D)** Acipenseriformes *Errolichthys* sp., CUGM 00346, Gujiao. **(E)** Palaeonisciformes indet., CUGM 00347, Gujiao. **(F)** Perleidiformes *Teffichthys elegans*, CUGM 00348, Gujiao. **(G–H)** Hybodontiformes tooth, Gujiao, (G) CUGM 00349, (H) CUGM 00350.

**Fig. 3. Invertebrates from the Guiyang Biota. (A)** Ammonoid *Pseudosageceras* sp., CUGM 00351, Gujiao. **(B)** Ammonoid *Radioceras* sp., CUGM 00352, Lianhuachun. **(C)** Bivalve *Eumorphotis hinnitidae*, CUGM 00353, Gujiao. **(D)** Bivalve *Scythentolium* sp., CUGM 00354, Xiaba. **(E–G)** Shrimp Aegeridae indet., CUGM 00355, Baishuilong, under natural light (E), fluorescence photograph (F), μXRF phosphorus elemental map (G). **(H, I)** Shrimp Aegeridae indet., CUGM 00356, Baishuilong, under natural light (H), fluorescence photograph (I). **(J, K)** Shrimp *Anisaeger* sp., CUGM 00357, Baishuilong, under natural light

(J), composite multispectral imaging (K). **(L)** Litogastrid lobster, CUGM 00358, Xiaba. **(M, N)** Cyclida, CUGM 00359, Xiaba section, under natural light (M), μXRF phosphorus elemental map (N). **(O)** Coprolites, CUGM 00360, Gujiao. **(P)** Foraminifer *Postcladella kalhori,* CUGM 00361, Gujiao. **(Q)** Sponge spicule, CUGM 00362, Gujiao. Scale bars in (P) and (Q) represent 100 μm.

**Fig. 4. Taxonomic and ecological features of the Guiyang biota and comparison with other main biotas after the PTME. (A)** Number of major groups and ecological categories of main Triassic biotas. See Fig. S12 for the definition of ecological categories. The fossil data for each biota are available in Data S1. Vertical bars indicate 95% confidence intervals based on rarefaction analyses (n = 25). **(B)** Taxonomic composition and species richness of the main Triassic biotas. The lack of Permian Lagerstätte (*44*) prevents a direct comparison of Lagerstätten before and after the PTME. **(C)** Previously hypothesized trophically stepwise model of the recovery after the PTME (*7*). The Dienerian Guiyang Biota highly contrasts with this model. From bottom to top, the trophic levels are primary producers (PP), such as algae; primary consumers (PC), such as foraminifers and sponges; meso-consumers (MC), such as bivalves and brachiopods; predatory invertebrates (P1), such as ammonoids and decapods; and predatory fishes and reptiles (P2). **(D)** Artistic reconstruction of the Guiyang Biota. Produced by Dinghua Yang. Wu. Wuchiapingian, C. Changhsingian, I. Induan (= Griesbachian + Dienerian), Ol. Olenekian (= Smithian + Spathian), La. Ladinian.

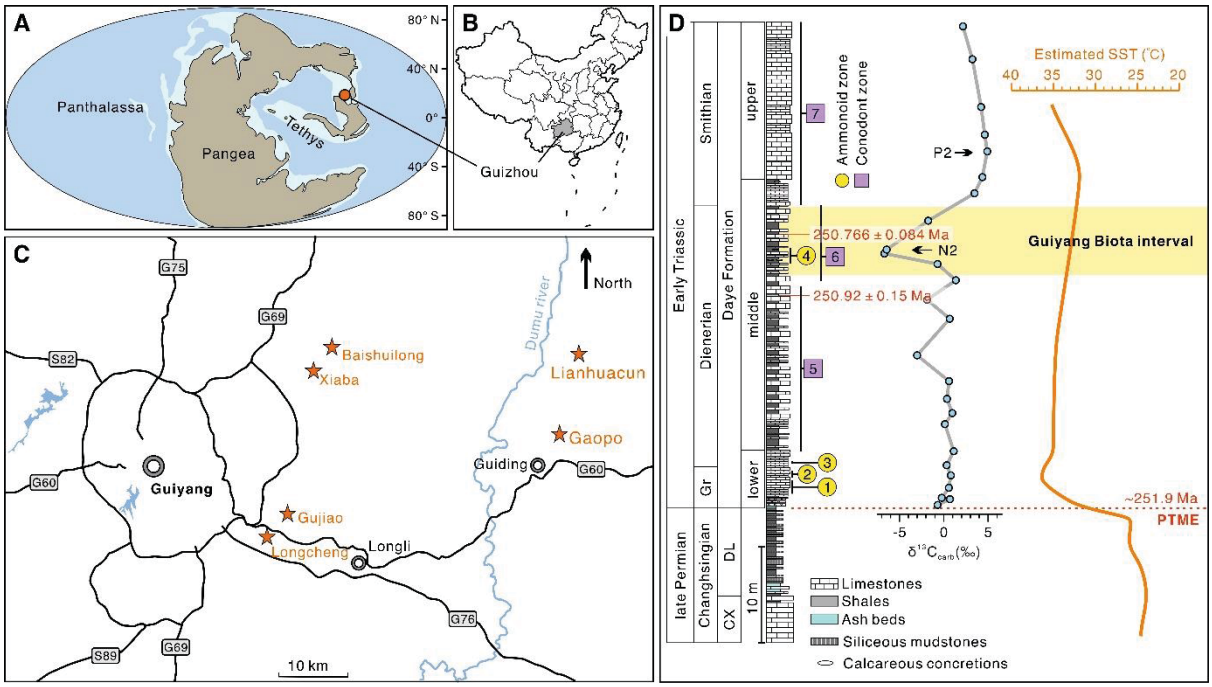


**Fig. 1. Geological context of the Guiyang Biota. (A–C)** Early Triassic and present-day locations of the studied exposures. Early Triassic paleogeographic map was modified from Scotese (*42*). **(D)** Synthetic regional lithological succession with associated carbon isotopic trend (analyzed in this study) and simplified estimated sea surface temperature (SST) modified from Sun et al. (*20*). Gr: Griesbachian, CX: Changxing Formation, DL: Dalong Formation. The yellow band indicates the stratigraphic position of the Guiyang Biota. Ammonoid zonation after Dai et al. (*43*): 1, *Ophiceras medium* beds; 2, *Jieshaniceras guizhouense* beds; 3, *Ambites radiatus* bed; 4, *Radioceras* sp. beds. Conodont zones: 5, *Neospathodus dieneri* Zone; 6, *Neospathodus cristagalli* Zone; 7, *Novispathodus waageni* Zone. The definitions of N2 and P2 of the carbon isotope curve refer to Song et al. (*26*).

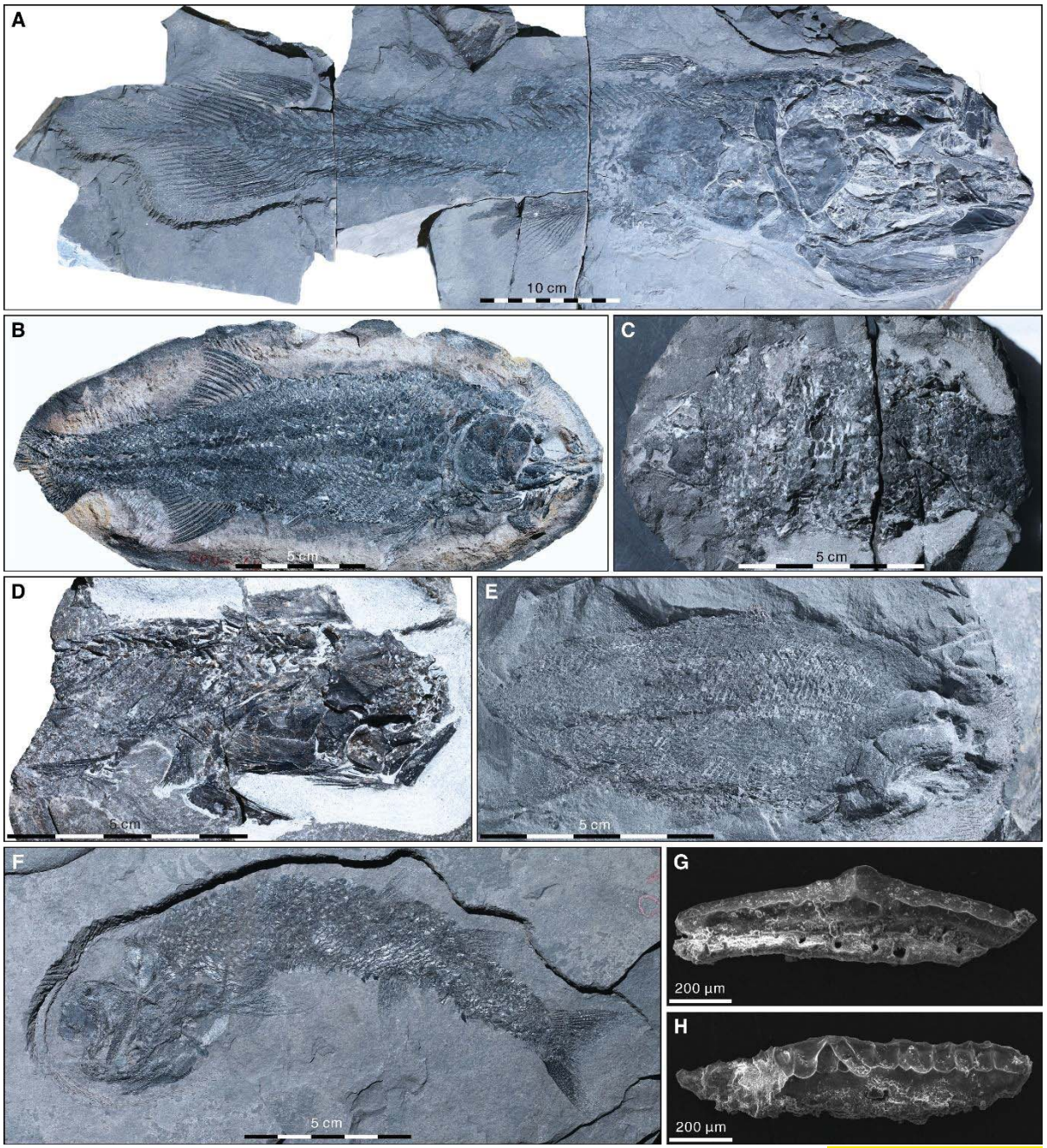


**Fig. 2. Osteichthyes and Chondrichthyes from the Guiyang Biota. (A)** Coelacanthiformes indet. A, CUGM 00343, Gujiao. **(B)** Parasemionotiformes *Watsonulus* sp., CUGM 00344, Gaopo. **(C)** Polzbergiformes indet., CUGM 00345, Gujiao. **(D)** Acipenseriformes *Errolichthys* sp., CUGM 00346, Gujiao. **(E)** Palaeonisciformes indet., CUGM 00347, Gujiao. **(F)** Perleidiformes *Teffichthys elegans*, CUGM 00348, Gujiao. **(G–H)** Hybodontiformes tooth, Gujiao, (G) CUGM 00349, (H) CUGM 00350.

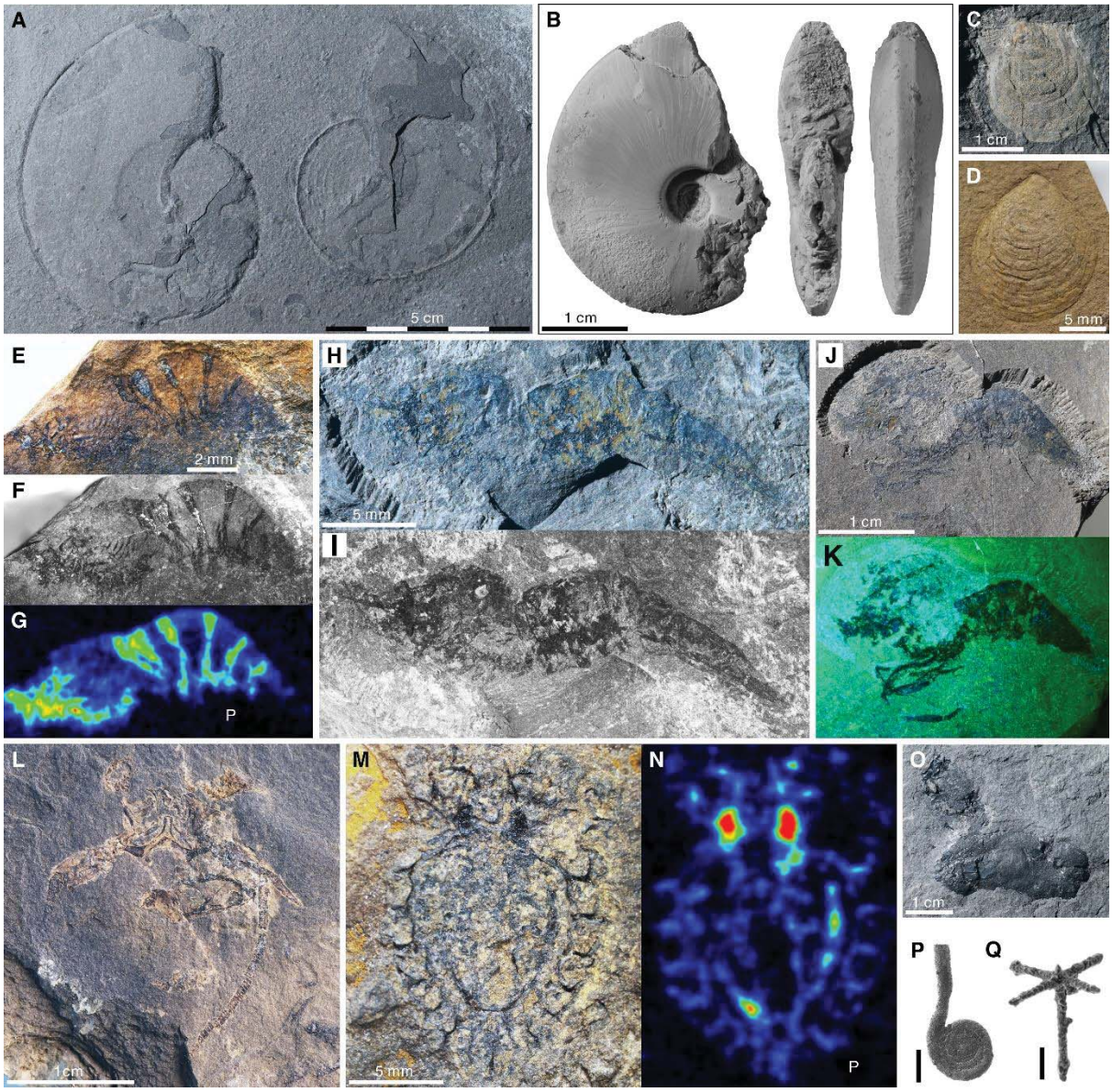


**Fig. 3. Invertebrates from the Guiyang Biota. (A)** Ammonoid *Pseudosageceras* sp., CUGM 00351, Gujiao. **(B)** Ammonoid *Radioceras* sp., CUGM 00352, Lianhuachun. **(C)** Bivalve *Eumorphotis hinnitidae*, CUGM 00353, Gujiao. **(D)** Bivalve *Scythentolium* sp., CUGM 00354, Xiaba. **(E–G)** Shrimp Aegeridae indet., CUGM 00355, Baishuilong, under natural light (E), fluorescence photograph (F), µXRF phosphorus elemental map (G). **(H, I)** Shrimp Aegeridae indet., CUGM 00356, Baishuilong, under natural light (H), fluorescence photograph (I). **(J, K)** Shrimp *Anisaeger* sp., CUGM 00357, Baishuilong, under natural light (J), composite multispectral imaging (K). **(L)** Litogastrid lobster, CUGM 00358, Xiaba. **(M, N)** Cyclida, CUGM 00359, Xiaba section, under natural light (M), µXRF phosphorus elemental map (N). **(O)** Coprolites, CUGM 00360, Gujiao. **(P)** Foraminifer *Postcladella kalhori*, CUGM 00361, Gujiao. **(Q)** Sponge spicule, CUGM 00362, Gujiao. Scale bars in (P) and (Q) represent 100 µm.

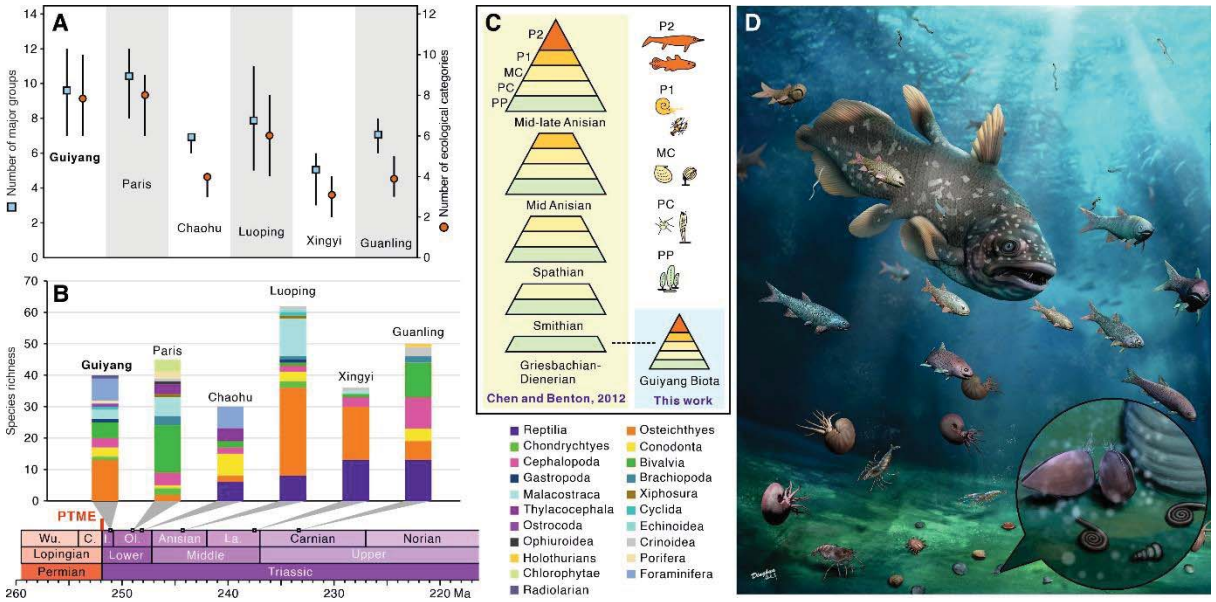


**Fig. 4. Taxonomic and ecological features of the Guiyang biota and comparison with other main biotas after the PTME. (A)** Number of major groups and ecological categories of main Triassic biotas. See Fig. S12 for the definition of ecological categories. The fossil data for each biota are available in Data S1. Vertical bars indicate 95% confidence intervals based on rarefaction analyses (n = 25). **(B)** Taxonomic composition and species richness of the main Triassic biotas. The lack of Permian Lagerstätte (*44*) prevents a direct comparison of Lagerstätten before and after the PTME. **(C)** Previously hypothesized trophically stepwise model of the recovery after the PTME (*7*). The Dienerian Guiyang Biota highly contrasts with this model. From bottom to top, the trophic levels are primary producers (PP), such as algae; primary consumers (PC), such as foraminifers and sponges; meso-consumers (MC), such as bivalves and brachiopods; predatory invertebrates (P1), such as ammonoids and decapods; and predatory fishes and reptiles (P2). **(D)** Artistic reconstruction of the Guiyang Biota. Produced by Dinghua Yang. Wu. Wuchiapingian, C. Changhsingian, I. Induan (= Griesbachian + Dienerian), Ol. Olenekian (= Smithian + Spathian), La. Ladinian.

Science
AAAS

# Supplementary Materials for

## A Mesozoic fossil lagerstätte from 250.8 Ma showing a modern-type marine ecosystem

Xu Dai, Joshua H.F.L. Davies, Zhiwei Yuan, Arnaud Brayard, Maria Ovtcharova, Guanghui Xu, Xiaokang Liu, Christopher P.A. Smith, Carrie E. Schweitzer, Mingtao Li, Morgann G. Perrot, Shouyi Jiang, Luyi Miao, Yiran Cao, Jia Yan, Ruoyu Bai, Fengyu Wang, Wei Guo, Huyue Song, Li Tian, Jacopo Dal Corso, Yuting Liu, Daoliang Chu, Haijun Song*

Correspondence to: haijunsong@cug.edu.cn

**This PDF file includes:**



**Other Supplementary Materials for this manuscript include the following:**

## Materials and Methods

### Provenance of the studied specimen

More than 1000 specimens were collected from six sections (Gujiao, Longcheng, Gaopo, Lianhuacun, Xiaba, and Baishuilong) near Guiyang (Fig. 1). All studied specimens are housed at the Yifu Museum of China University of Geosciences (CUGM). The age of these fossils was determined to the late Dienerian (~250.8 Ma, Early Triassic) based on ammonoid and conodont biostratigraphy, carbon isotope chemostratigraphy, and high-precision U-Pb dating. See **Age of the Guiyang Biota** section for detailed information. For the abbreviations of the collectors refer to **Author contribution** section.

| Name | Register No. | Section | Collector |
|---|---|---|---|
| **Coelacanthiformes indet. A** | CUGM 00343 | Gujiao | XD, XL, LM |
| ***Watsonulus* sp.** | CUGM 00344 | Gaopo | XL |
| **Polzbergiformes indet.** | CUGM 00345 | Gujiao | XD, XL, LM |
| ***Errolichthys* sp.** | CUGM 00346 | Gujiao | XD, DC |
| **Palaeonisciformes indet.** | CUGM 00347 | Gujiao | XD, XL, LM |
| ***Teffichthys elegans*** | CUGM 00348 | Gujiao | ZY |
| **Hybodontiform tooth** | CUGM 00349 | Gujiao | ZY |
| **Hybodontiform tooth** | CUGM 00350 | Gujiao | ZY |
| ***Pseudosageceras* sp.** | CUGM 00351 | Gujiao | XD, XL, LM |
| ***Radioceras* sp.** | CUGM 00352 | Lianhuacun | XD, XL, RC |
| ***Eumorphotis hinnitidae*** | CUGM 00353 | Gujiao | XD, XL, LM |
| ***Scythentolium* sp.** | CUGM 00354 | Xiaba | XD, DC |
| **Aegeridae indet.** | CUGM 00355 | Baishuilong | XD, SJ |
| **Aegeridae indet.** | CUGM 00356 | Baishuilong | XD, SJ |
| ***Anisaeger* sp.** | CUGM 00357 | Baishuilong | XD, SJ |
| **Litogastrid lobster** | CUGM 00358 | Xiaba | XD |
| **Cyclida** | CUGM 00359 | Xiaba | DC, XD |
| **Coprolites** | CUGM 00360 | Gujiao | XD, XL, LM |
| ***Postcladella kalhori*** | CUGM 00361 | Gujiao | XD |
| **Sponge spicule** | CUGM 00362 | Gujiao | ZY |
| ***Eurygnathodus costatus*** | CUGM 00363 | Gujiao | RB |
| ***Eurygnathodus costatus*** | CUGM 00364 | Gujiao | RB |
| ***Neospathodus cristagalli*** | CUGM 00365 | Gujiao | RB |
| ***Neospathodus dieneri*** | CUGM 00366 | Gujiao | RB |
| ***Novispathodus waageni*** | CUGM 00367 | Gujiao | RB |
| ***Novispathodus waageni*** | CUGM 00368 | Gujiao | RB |
| ***Novispathodus posterolongatus*** | CUGM 00369 | Gujiao | RB |

| | | | |
|---|---|---|---|
| **Coelacanthiformes indet. B** | CUGM 00370 | Longcheng | XD, XL |
| ***Boresomus* sp.** | CUGM 00371 | Gujiao | XD, XL, LM |
| ***Errolichthys* sp.** | CUGM 00372 | Gaopo | XD, XL, LM, YC |
| **Actinopterygii indet. B** | CUGM 00373 | Gujiao | XD, XL, LM |
| **Actinopterygii indet. E** | CUGM 00374 | Gaopo | XD, XL, LM, YC |
| **Aegeridae indet.** | CUGM 00375 | Baishuilong | XD, SJ |
| **Aegeridae indet.** | CUGM 00376 | Baishuilong | XD, SJ |
| **Aegeridae indet.** | CUGM 00377 | Baishuilong | XD, SJ |
| **Aegeridae indet.** | CUGM 00378 | Baishuilong | XD, SJ |
| **Aegeridae indet.** | CUGM 00379 | Baishuilong | XD, SJ |
| ***Pseudosageceras* sp.** | CUGM 00380 | Gujiao | XD, XL, LM |
| **Ammonoid indet.** | CUGM 00381 | Gujiao | XD, XL, LM |
| ***Eumorphotis* sp.** | CUGM 00382 | Gujiao | XD, XL, LM |
| ***Eumorphotis hinnitidae*** | CUGM 00383 | Gujiao | XD, XL, LM |
| ***Modiolus* sp.** | CUGM 00384 | Gaopo | XD, XL, LM, YC |
| ***Nodosinelloides aequiampla*** | CUGM 00385 | Gujiao | XD |
| ***Planiinvoluta* sp.** | CUGM 00386 | Gujiao | XD |
| ***Tezaquina* sp.** | CUGM 00387 | Gujiao | XD |
| ***Rectostipulina quadrata*** | CUGM 00388 | Gujiao | XD |
| ***Postcladella kalhori*** | CUGM 00389 | Gujiao | XD |
| ***Postcladella kalhori*** | CUGM 00390 | Gujiao | XD |
| ***Postcladella kalhori*** | CUGM 00391 | Gujiao | XD |
| **Sponge spicule** | CUGM 00392 | Gujiao | ZY |
| ***Latentifistula* sp.** | CUGM 00393 | Gujiao | YL |

## Fossil preparation

Mechanical preparation was carefully carried out under a microscope using air scribes to work out anatomical details of fishes, ammonoids, bivalves, and shrimps to facilitate their taxonomic assignments.

Thirty-six, 37, and 18 samples of limestones and calcareous concretions were taken from Gujiao, Baishuilong, and Gaopo sections, respectively, and thin-sectioned for foraminifer study and microfacies analysis.

Ten samples of limestone and calcareous concretion, with an average weight of 5 kg, were taken from the fossiliferous interval at the Gujiao section. They were dissolved in 10% acetic acid after a coarse crushing into ~2 $cm^3$-size fragments. After filtering through 20-mesh and 160-mesh sieves, the residues were separated in 2.78–2.80 g/ml heavy liquid.

Conodonts were carefully selected under a stereomicroscope and well-preserved conodonts were picked out to be photographed using a scanning electronic microscope (Quanta200, SU8010) at the School of Earth Sciences, China University of Geosciences, Wuhan.

**Macrofossil Imaging**

Macrofossil specimens were photographed under natural light and UV light using a Canon 70D camera with a Micro EF lens with 100 mm focal length and f/2.8 aperture. We tested three different UV-light wave lengths: 310, 365 and 410 nm. Unfortunately, no specimens from the Guiyang Biota reacted under UV-light.

Fluorescence images were taken using a Leica DFC340 FX monochrome digital camera attached to a Leica M205 FA fluorescence stereomicroscope (green-orange fluorescence) at Yunnan Key Laboratory for Palaeobiology, Yunnan University.

The elemental maps were obtained using the M4 Tornado micro-XRF (Bruker, USA) which permits large surface scanning with a lateral resolution up to 50 µm. The analysis was performed at the Qingdao Sparata Analysis & Test Co., Ltd. The M4 micro-XRF consists of a mobile measuring head that can scan the surface of a sample on an XY-motorized stage. The operating conditions are listed in Table S6.

**SEM-EDS**

Pyritized foraminifers, fish scales and coprolites were observed and photographed using a scanning electronic microscope (SEM, HITACHI-SU8010). Energy Dispersive X-ray Spectrometry (EDS) was used for elemental analyses. All these analyses were conducted at the State Key Laboratory of Biogeology and Environmental Geology, China University of Geosciences (Wuhan).

**Biostratigraphy**

Three conodont species were found in the fossiliferous interval at Gujiao, *Neospathodus cristagalli*, *Neospathodus dieneri*, and *Novispathodus posterolongatus*. This assemblage corresponds to the *Ns. dieneri-Ns. cristagalli* Zone at Meishan (*45*) and the *Ns. cristagalli* Zone at Bianyang (*46*). It indicates a Dienerian age. Similar associations also occur in the Dienerian of the Salt Range, Pakistan (*21*) and British Columbia (*47*). A second conodont assemblage, ~2 m above the Guiyang Biota, is dominated by *Eurygnathodus costatus* and *Novispathodus waageni*, suggesting an early Smithian age (*48*).

Ammonoids from the Guiyang Biota are usually poorly preserved as 2D imprints in black shale layers. These often resemble the long-ranging Dienerian-Spathian genus *Pseudosageceras*. However, a few specimens preserved in 3D within carbonate concretions can be identified as *Radioceras* sp. *Radioceras* ranges from the late Dienerian to the early Smithian in the Himalaya regions (*49*), and thus, well supports a Dienerian age assignment for the Guiyang Biota.

**Carbon isotopes**

Twenty-six limestone samples were taken from the Gujiao section for carbon isotope analysis. Carbonate carbon isotopes ($\delta^{13}C$) were prepared by drilling 1 mg of powder from the surface of a fresh sample. Approximately 0.4 mg powder was put in a 10 mL Na-glass vial, sealed with a butyl rubber septum, flushed with helium and then reacted with 100% phosphoric acid at 72 °C after. The carbon dioxide gas was analyzed for $\delta^{13}C$ using a MAT 253 mass-spectrometer coupled directly to a Finnigan Gasbench II interface (Thermo Scientific) at the State Key Lab of Biogeology and Environmental Geology (BGEG) in China University of Geosciences (Wuhan). The $\delta^{13}C$ values are presented as per mile (‰) relative to the Vienna Pee Dee Belemnite (V-PDB) standard. The analytical precision was better than 0.1‰ by repeating the analyses of two laboratory standards (GBW 04416 and GBW 04417).

**Zircon analyses**

Two ash layers were sampled at Gujiao, GJ-ASH-134 and GJ-ASH-157. Zircon was extracted from the ash samples at the China University of Geosciences, Wuhan using conventional separation techniques. The selected zircon crystals were then mounted, polished, and imaged on a scanning electron microscope (SEM) with a cathodoluminescence detector and analyzed by laser ablation inductively coupled mass spectrometry (LA-ICP-MS) to ensure that the grains were mostly volcanic autocrysts. Following LA-ICP-MS, selected zircon grains were removed from the mounts at the Geotop labs in the Université du Québec in Montreal and annealed in quartz crucibles for 48 h in a muffle furnace at 950 °C to partially anneal their radiation damage. After annealing, the grains were chemically abraded in concentrated HF at 210 °C for 12 h (*50*). After chemical abrasion, the zircons were sent to the University of Geneva for dissolution and mass spectrometry (following closely the techniques of Widmann et al. (*50*) where they were ultrasonically cleaned in 7N $HNO_3$ and then spiked with ~5 mg of the EARTHTIME $^{202}Pb$+$^{205}Pb$+$^{233}U$+$^{235}U$ tracer solution (*51*, *52*). The grains were then dissolved in pre-cleaned Savillex Microcapsules placed inside a Parr

digestion vessel, with 70 µl of concentrated HF. After digestion, the U and Pb fractions were separated using anion exchange columns. The aliquots of U and Pb were then loaded onto outgassed zone-refined Re filaments and placed into a Thermo Scientific TRITON. Pb was measured in dynamic peak jumping mode using a secondary electron multiplier, whereas $UO_2$ was measured either in static mode using Faraday cups attached $10^{13}$ Ω resistors or when the $UO_2$ signal was small the electron multiplier was used in dynamic peak jumping mode. All common Pb was attributed to laboratory blank and was assigned the long-term isotopic composition of the Geneva procedural blank (*53*). All U-Pb data processing was conducted using the Tripoli and Redux software packages, following the algorithms of McLean et al. (*54*). Ages reported in the text are given without the additional uncertainty associated with the tracer calibration and uranium decay constants, although these extra sources of uncertainty are included in Table S2. All ages were corrected for initial $^{230}Th$ disequilibrium in the melt using a U/Th ratio of the magma of 3.5. Ages from each of the studied intervals were only calculated using concordant analysis, and the $^{206}Pb/^{238}U$ age of the youngest grain is considered to most closely represent the age of the ash. Resulting ages and the heights of the ashes and locations of the Guiyang Biota were then used to calculate an age-depth model, to determine the age of the Guiyang Biota using the Bchron model in R (*55*).

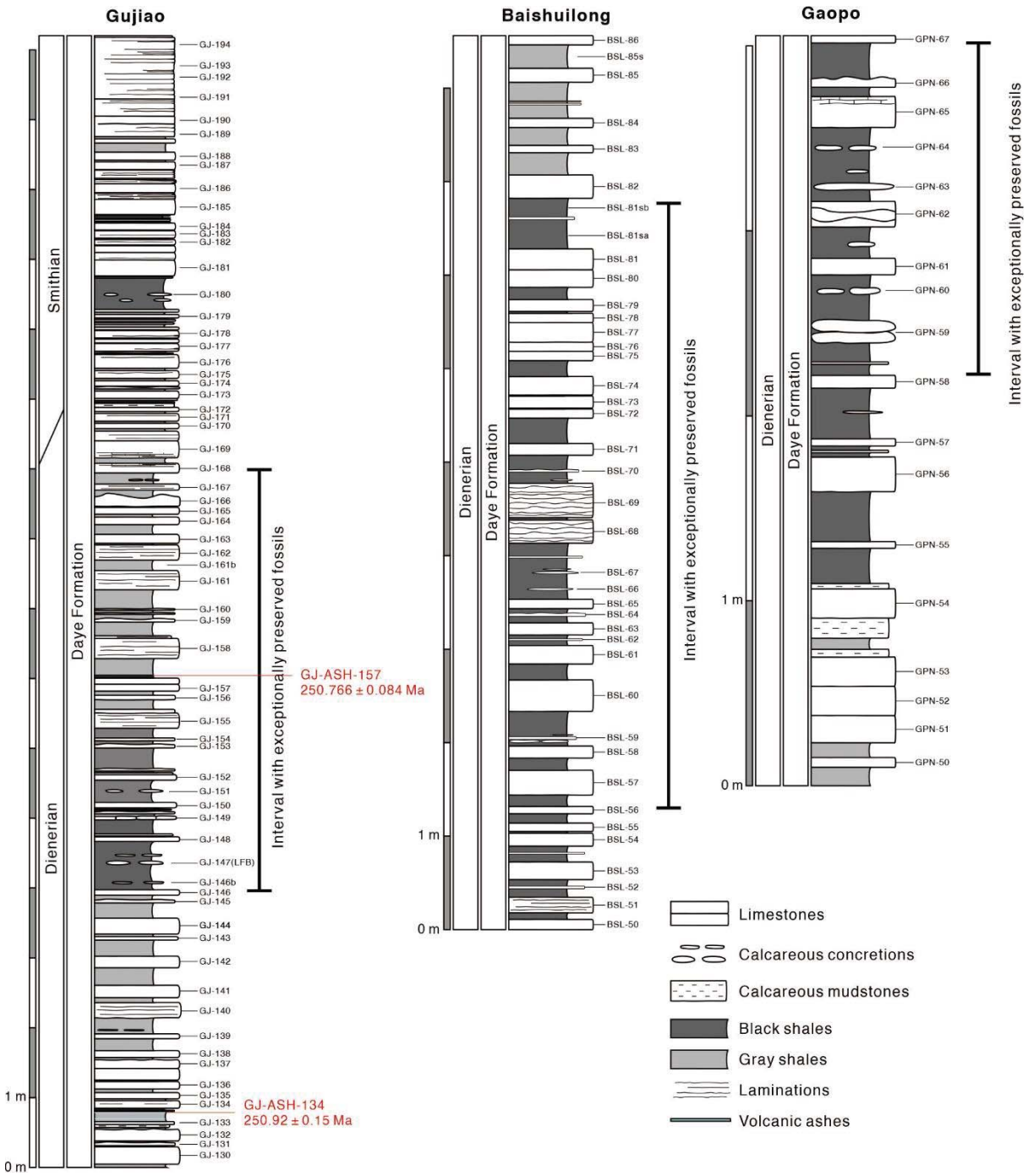


**Fig. S1. Detailed lithological logs of the studied sections.**

**Fig. S2. Outcrop photograph of the fossiliferous interval of the middle Daye Formation at the Gujiao section**, characterized by alternating finely-laminated black shales and thin-bedded, dark gray limestones.

**Fig. S3. Outcrop photograph of the fossiliferous interval of the middle Daye Formation at the Baishuilong section**, characterized by alternating finely-laminated black shales and thin- to medium-bedded gray limestones.

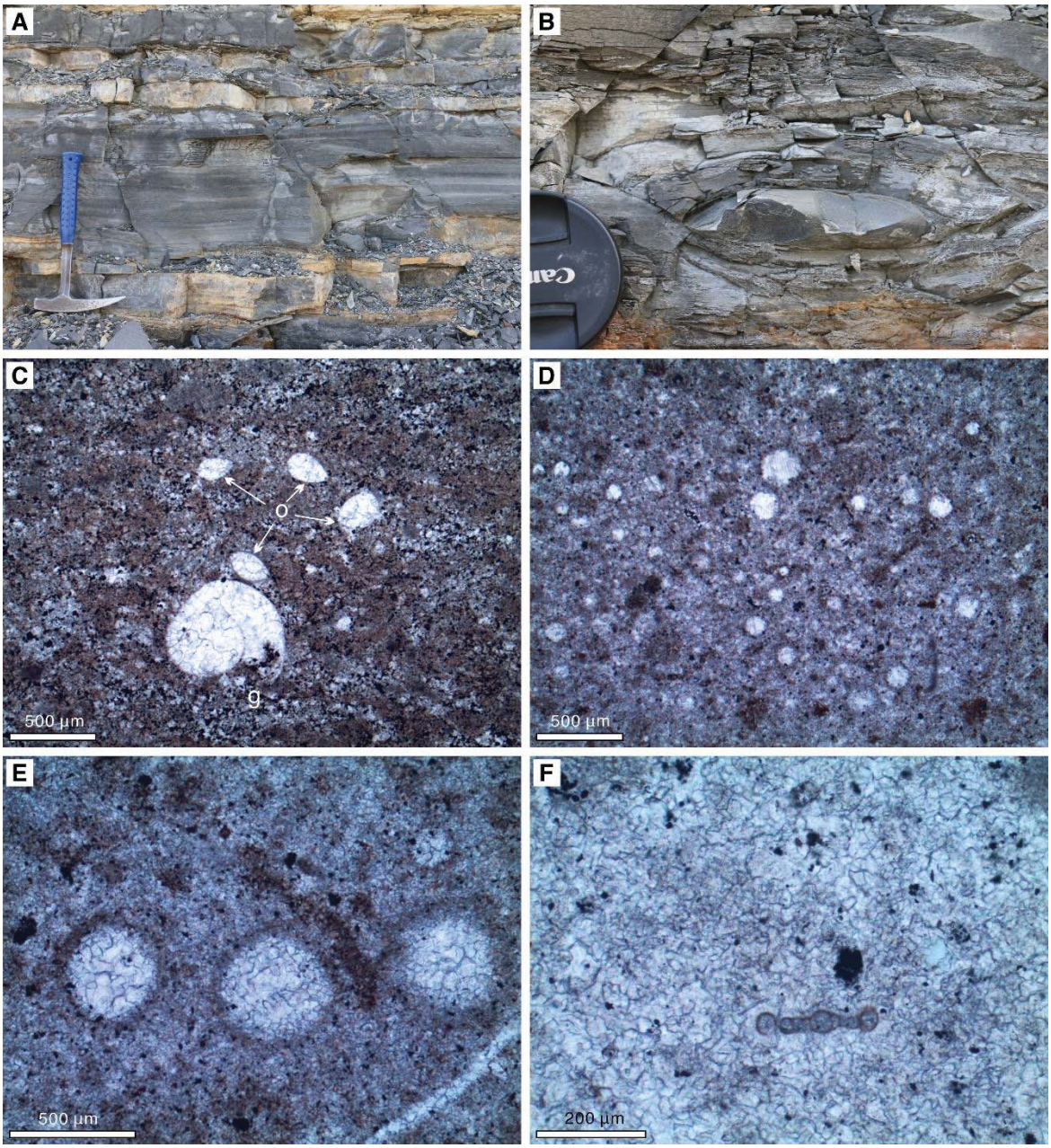


**Fig. S4. Outcrop photographs of the Gujiao section and thin-section views of samples collected at Gujiao**. **(A)** Close-up view of the middle unit of the Daye Formation containing the Guiyang Biota and showing thin-bedded limestones alternating with black shales. **(B)** Calcareous concretions intercalated in black shales. **(C)** Wackestone with ostracods (o) and gastropod (g), sample GJ-151. **(D)** Wackestone with microspheres and abundant small pyrite framboids scattered in the matrix, sample GJ-156. **(E)** Close-up view of the microspheres in sample GJ-156 showing an intense recrystallization. **(F)** Wackestone with a small specimen of the foraminifer *Postcladella kalhori* in sample GJ-159.

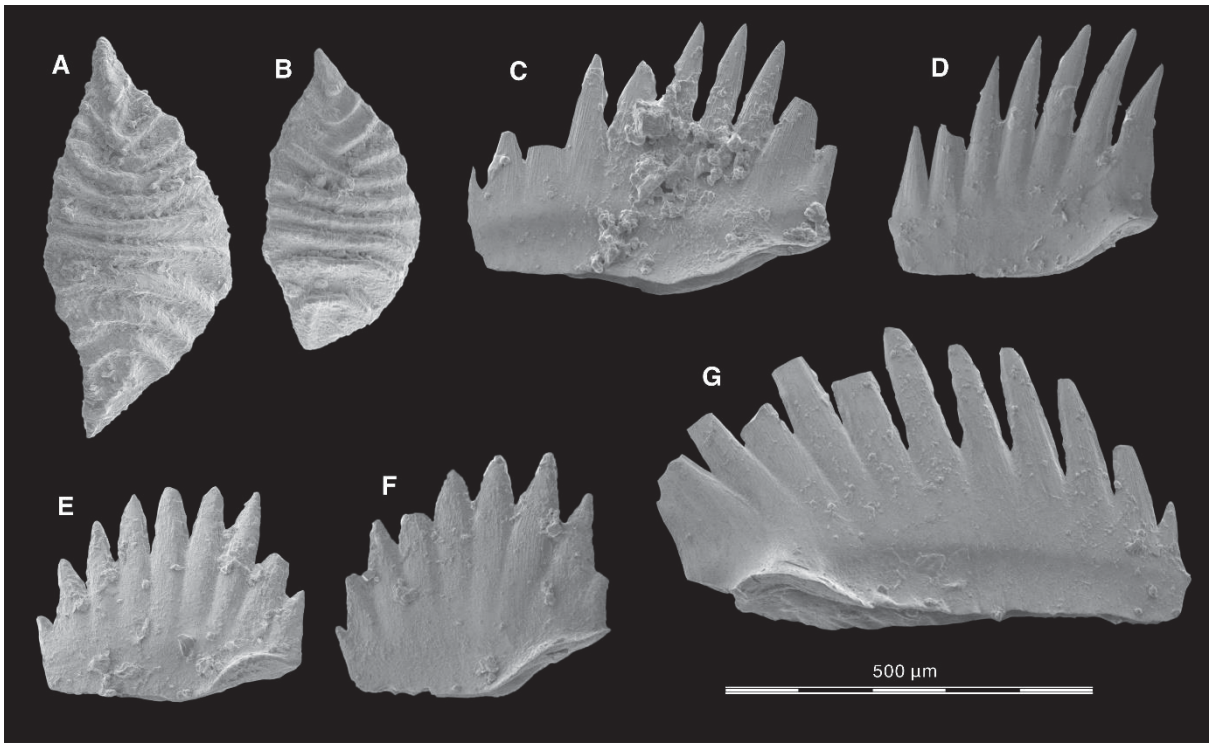


**Fig. S5. Age-diagnostic conodont species from the middle unit of the Daye Formation at the Gujiao section. (A-B)** *Eurygnathodus costatus*, (A) CUGM 00363, (B) CUGM 00364, from sample GJ-VI+20, oral view. **(C)** *Neospathodus cristagalli*, CUGM 00365, GJ-VI+0, lateral view. **(D)** *Neospathodus dieneri*, CUGM 00366, GJ-VI+8, lateral view. **(E-F)** *Novispathodus waageni*, (E) CUGM 00367, (F) CUGM 00368, from sample GJ-VI+20. **(G)** *Novispathodus posterolongatus*, CUGM 00369, from sample GJ-VI+0, lateral view.

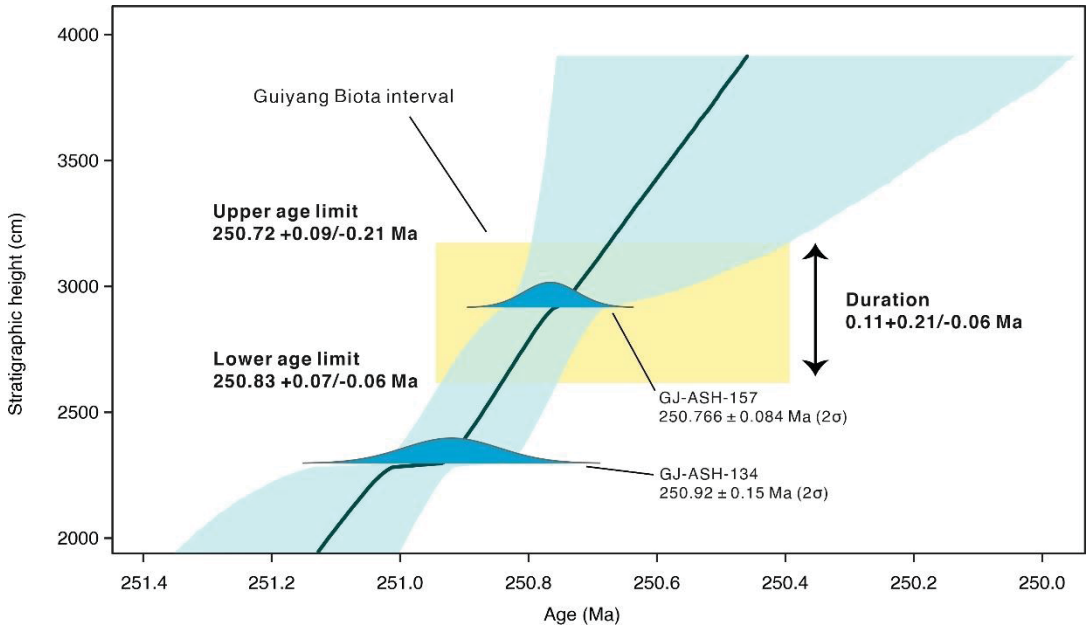


**Fig. S6. Age model of the Guiyang Biota.** Shade area represents 95% confidence interval. The height of the Permian/Triassic boundary in Gujiao section is marked as 0 cm. Note that in the latest version of the ICS International Chronostratigraphic Chart (v2022/10), the age of the Induan/Olenekian boundary (or the Dienerian/Smithian boundary) is 251.2 Ma, referring to Galfetti et al. *(56)*. This age was based on the ash sample CHIN40, from the early Smithian ammonoid *Kashmirites kapila* beds in Guangxi, South China. Later, Widmann et al. *(57)* re-analyzed this sample in the same lab, using the EarthTime gravimetrically calibrated tracer solution (*51*, *52*, ET2535, also used in this study) which allows accurate U and Pb mass fractionation correction and also an updated chemical abrasion procedure *(50)*, the resulting age was 250.647 ±0.064/0.09/0.28 Ma (2σ). This offset in age may be due to revised isotope tracer calibration and improved chemical abrasion procedures as explained *(50)*. However, this new age is missed in the latest International Chronostratigraphic Chart. Our dates are in good agreement with Widmann et al. *(57)*, suggesting a late Dienerian age for the Guiyang Biota.

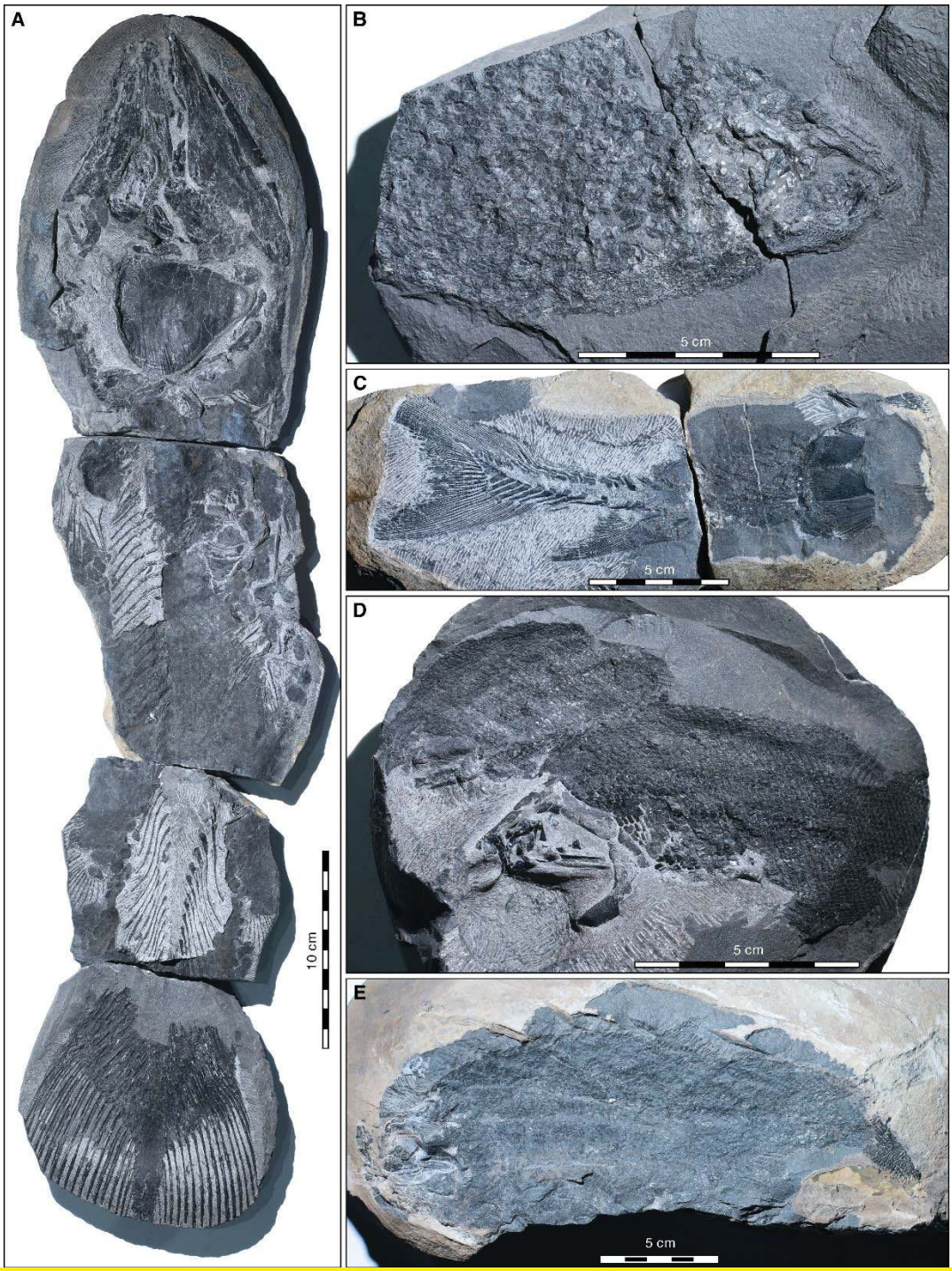


**Fig. S7. Fish fossils from the Guiyang Biota. (A)** Coelacanthiformes indet. B, CUGM 00370, from sample LC-31b, Longcheng. **(B)** Ptycholepiformes *Boresomus* sp., CUGM 00371, from sample GJ-151, Gujiao. **(C)** Acipenseriformes *Errolichthys* sp., CUGM 00372, Gaopo. **(D)** Actinopterygii indet. B, CUGM 00373, from sample GJ-147, Gujiao. **(E)** Actinopterygii indet. E, CUGM 00374, from sample GPN-60, Gaopo.

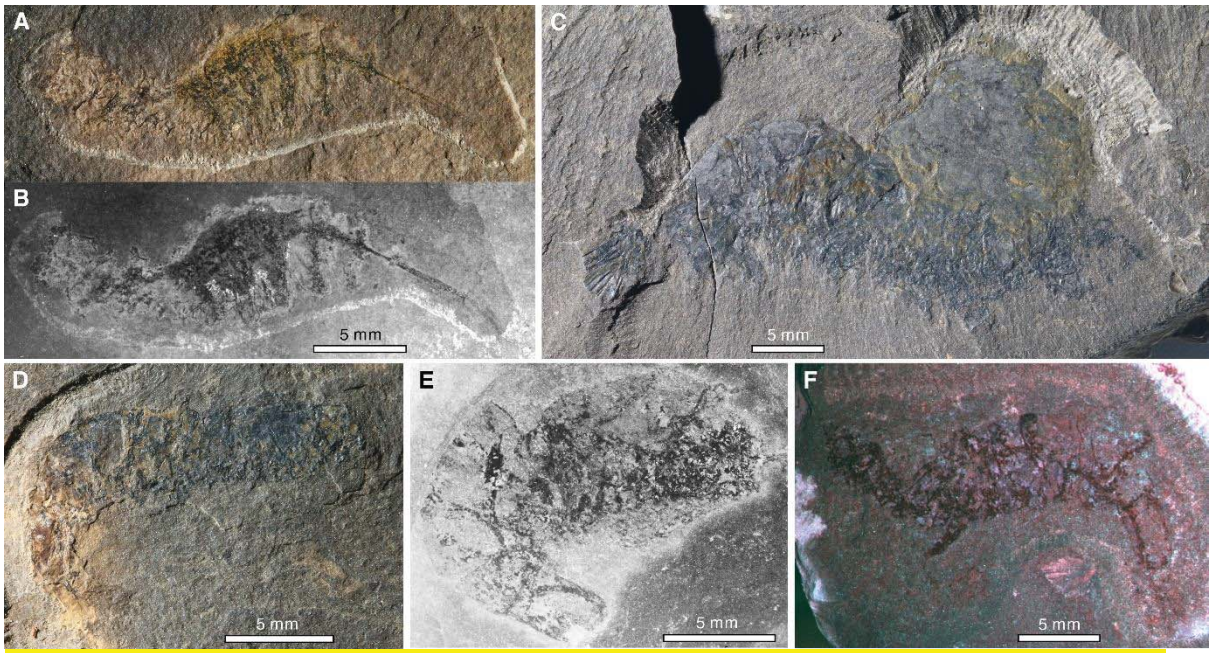


**Fig. S8. Aegeridae indet. from the Guiyang Biota, all from sample BSL-81SB. (A, B)** CUGM 00375, (A) under natural light, (B) fluorescence photograph. **(C)** CUGM 00376, under natural light**. (D)** CUGM 00377, under natural light**. (E)** CUGM 00378, fluorescence photograph. **(F)** CUGM 00379, composite multispectral image.

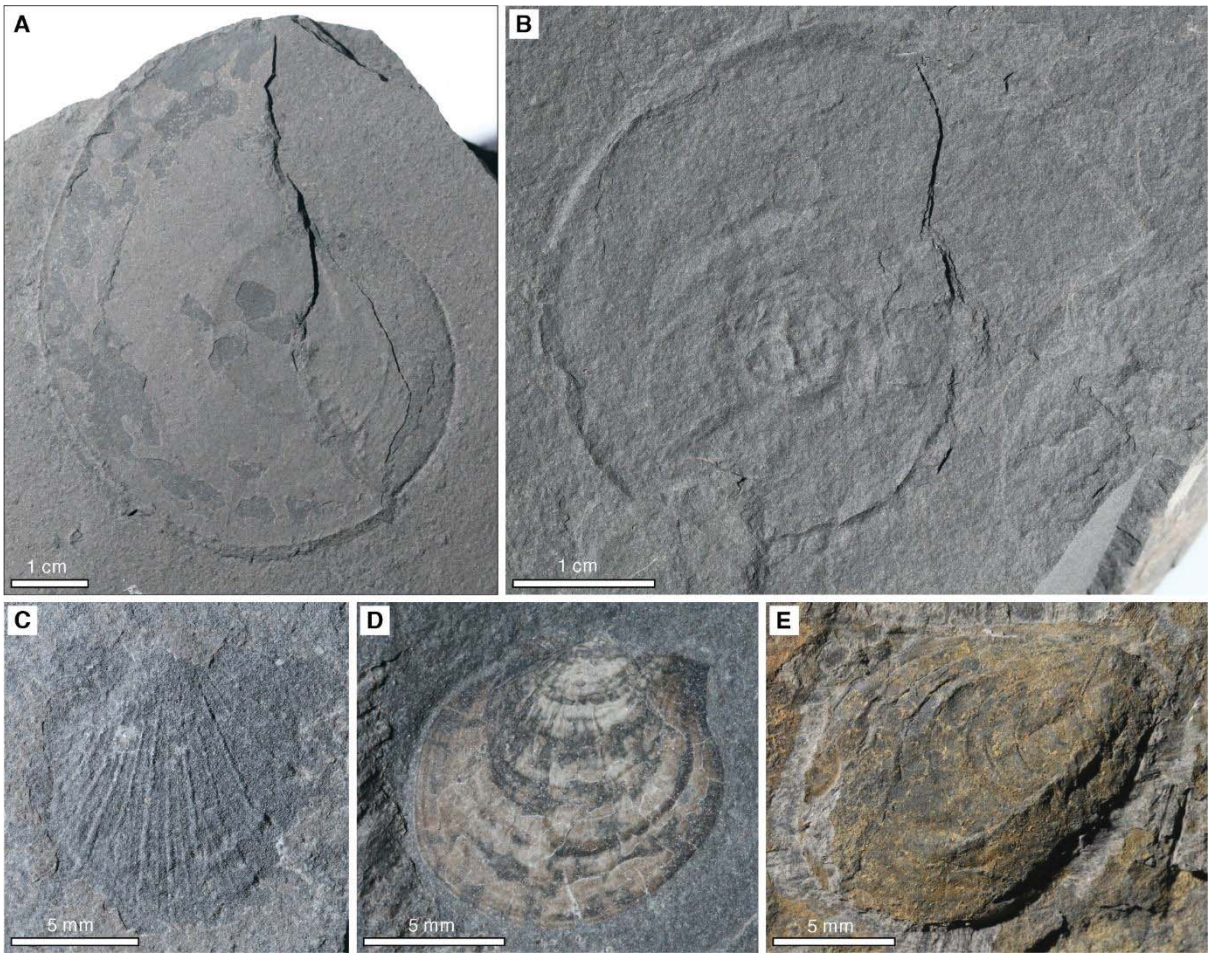


**Fig. S9. Mollusks from the Guiyang Biota. (A)** Ammonoid *Pseudosageceras* sp., CUGM 00380, from sample GJ-152b, Gujiao. **(B)** Ammonoid indet., CUGM 00381, from sample GJ-151, Gujiao. **(C)** Bivalve *Eumorphotis* sp., left valve, CUGM 00382, from sample GJ-161b, Gujiao,. **(D)** Bivalve *Eumorphotis hinnitidae*, right valve, CUGM 00383, from sample GJ-161b, Gujiao. **(E)** Bivalve *Modiolus* sp., right valve, CUGM 00384, from sample GPN-66b, Gaopo,.

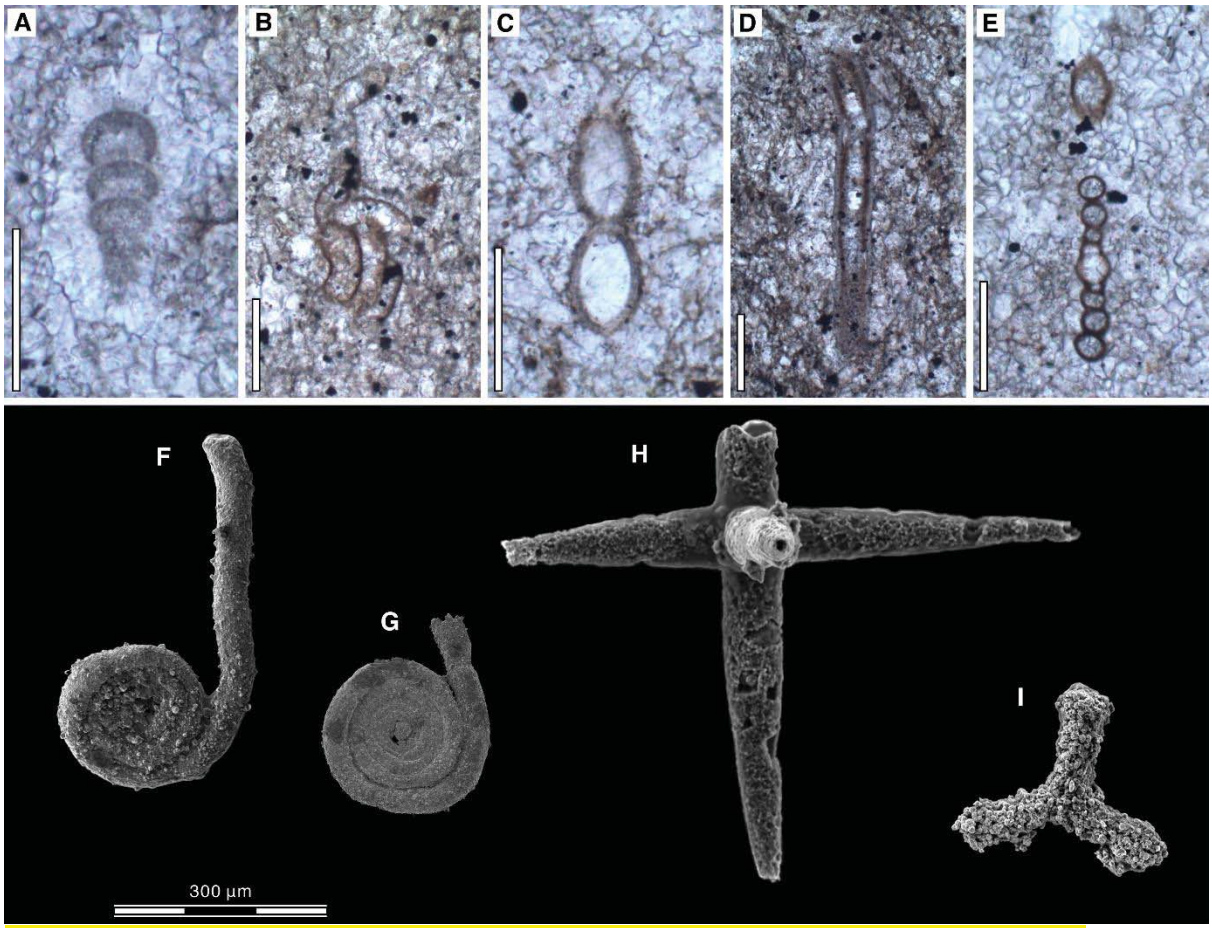


**Fig. S10. Microfossils from the Guiyang Biota, all from the Gujiao section. (A)** Foraminifer *Nodosinelloides aequiampla*, CUGM 00385, from sample GJ-168. **(B)** Foraminifer *Planiinvoluta* sp., CUGM 00386, from sample GJ-159. **(C)** Foraminifer *Tezaquina* sp., CUGM 00387, from sample GJ-163. **(D)** Foraminifer *Rectostipulina quadrata*, CUGM 00388, from sample GJ-163. **(E-G)** Foraminifer *Postcladella kalhori*. (E) CUGM 00389, from samples GJ-159, (F) CUGM 00390, from sample GJ-163, (G) CUGM 00391, from sample GJ-163. **(H)** Sponge spicule, CUGM 00392, from sample GJ-160. **(I)** Radiolarian *Latentifistula* sp., CUGM 00393, from sample GJ-158. Scales bars in A-E represent 100 µm.

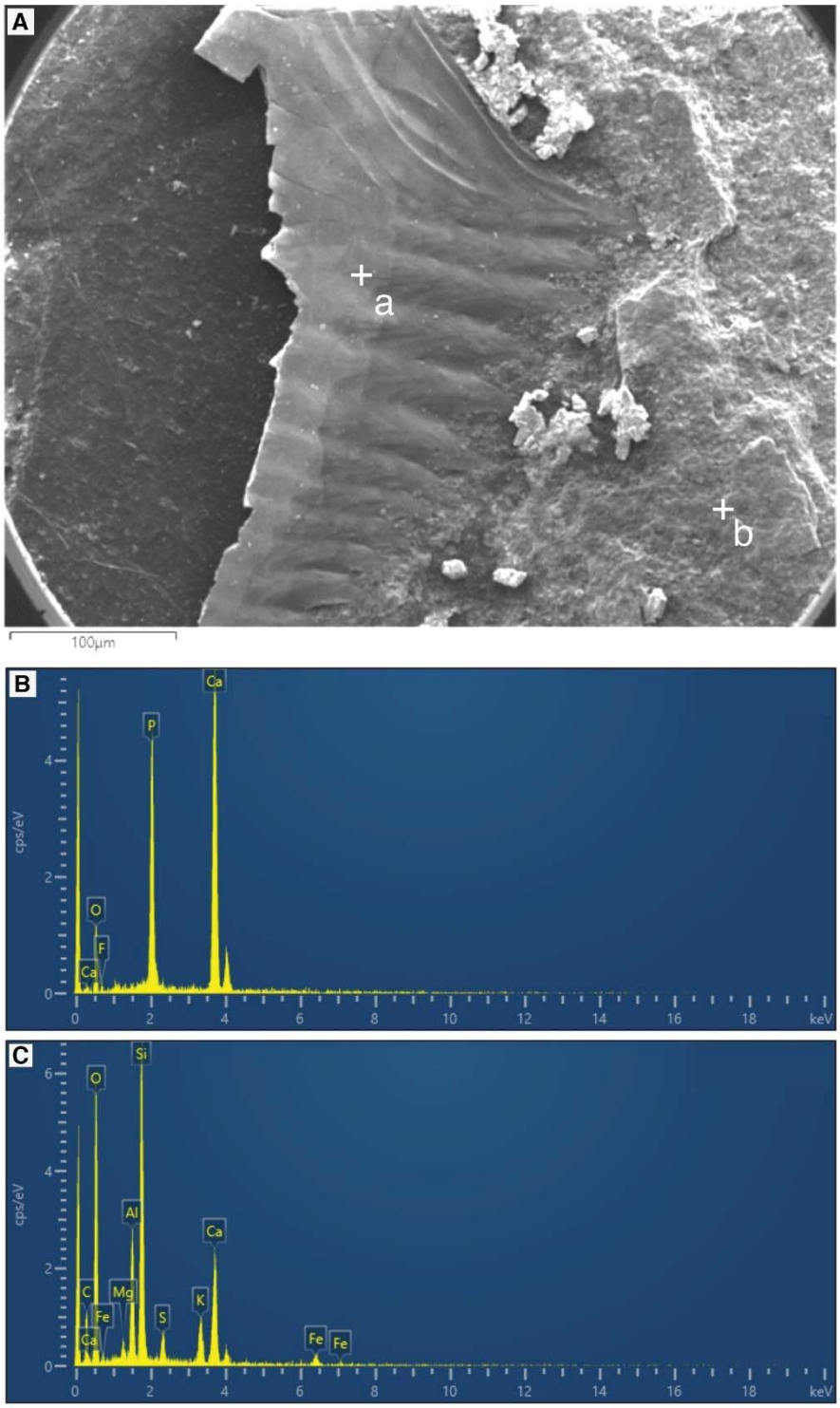


**Fig. S11. SEM photograph and EDS analyses for a fish scale and the surrounding matrix from sample GJ-151, Gujiao. (A)** SEM photograph of the fish scale, target points for EDS analyses indicated by **a** and **b**. **(B)** EDS analyses for target point **a** indicate that the fish scale is preserved in calcium phosphate. **(C)** EDS analyses for target point **b** show that the matrix is dominated by aluminosilicates.

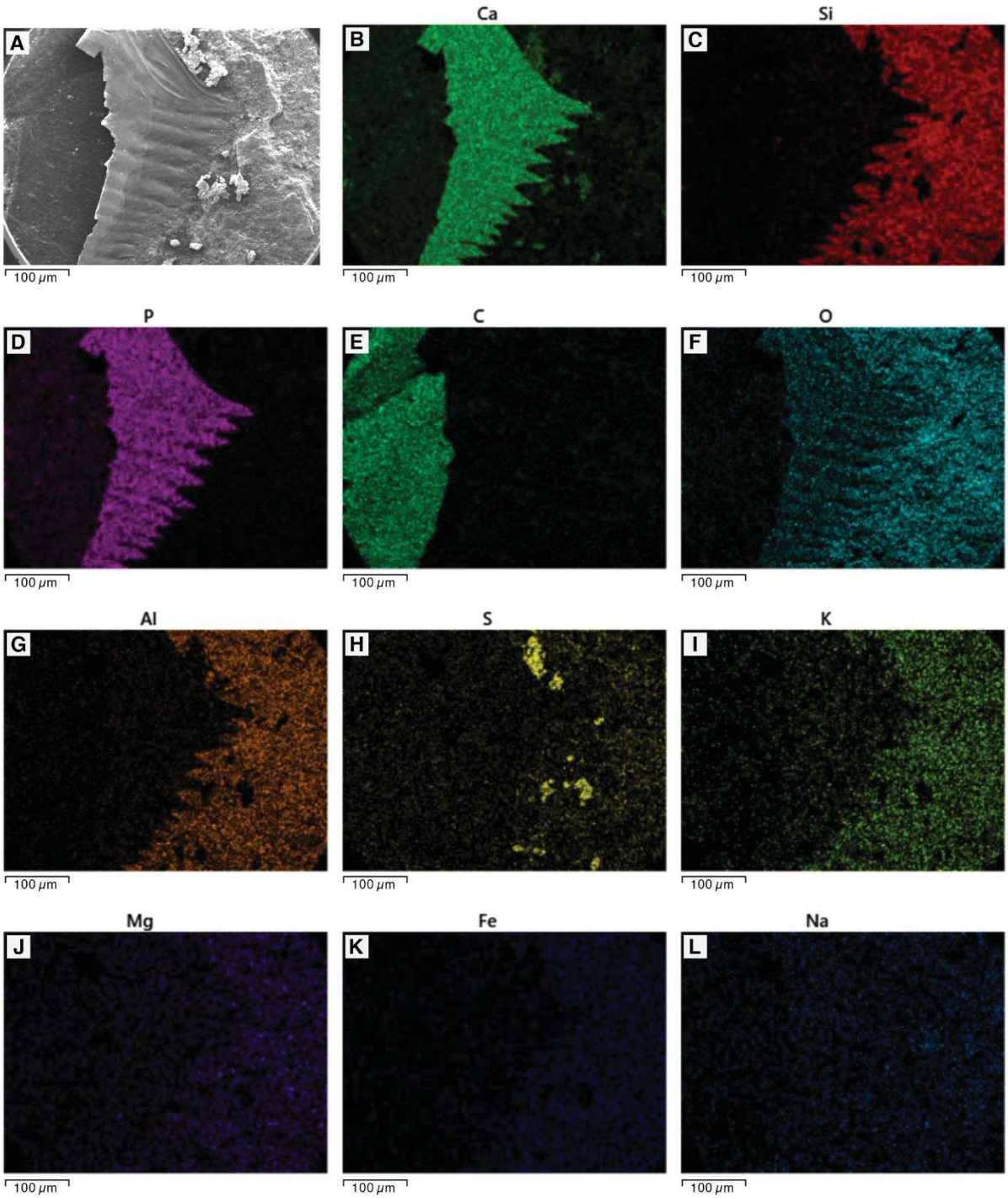


**Fig. S12. EDS elemental maps for the fish scale from sample GJ-151, Gujiao, indicating that it is preserved in calcium phosphate.**

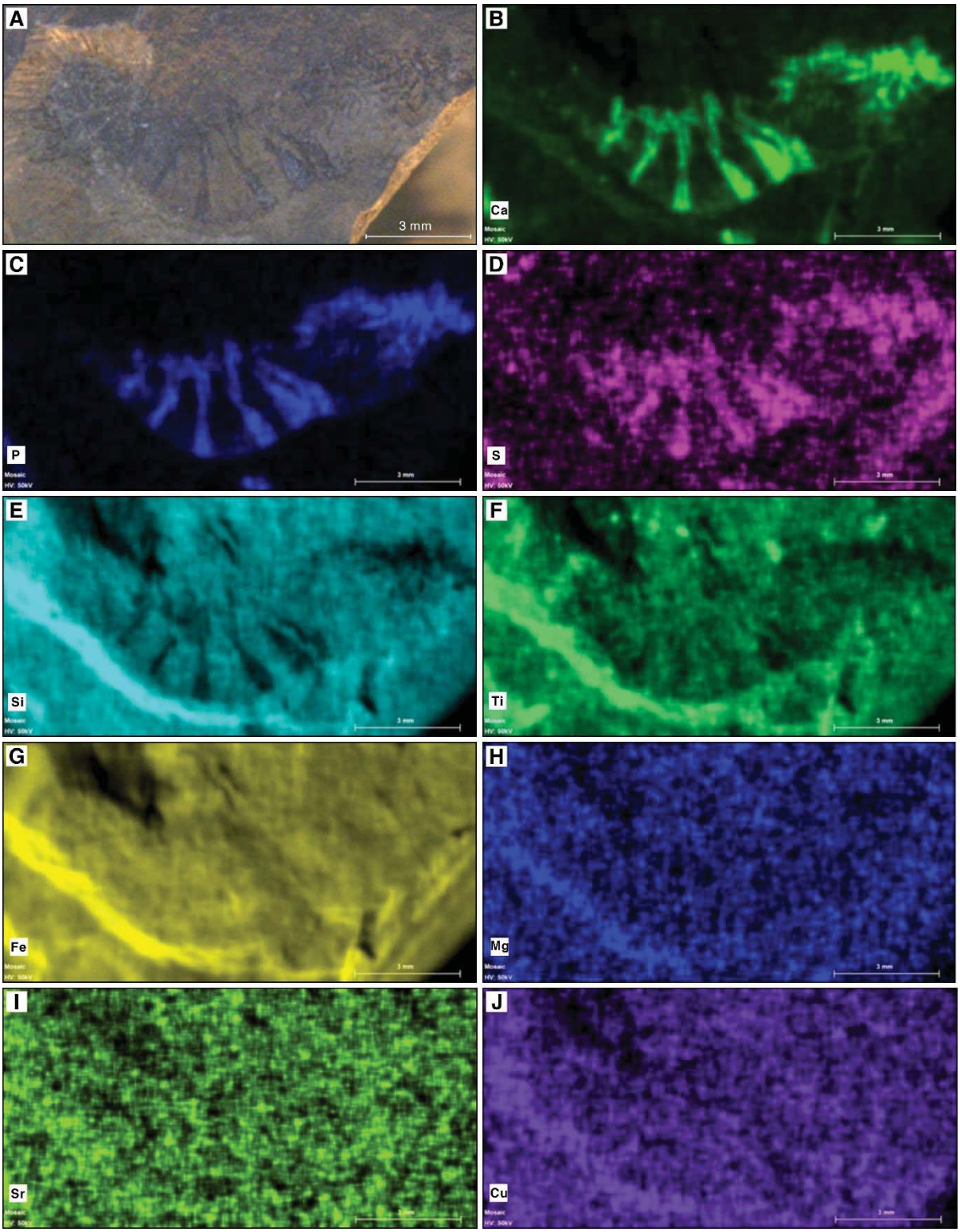


**Fig. S13. µXRF elemental maps for shrimp Aegeridae indet. from sample BSL-81SB, Baishuilong, showing that the specimen is preserved in calcium phosphate.**

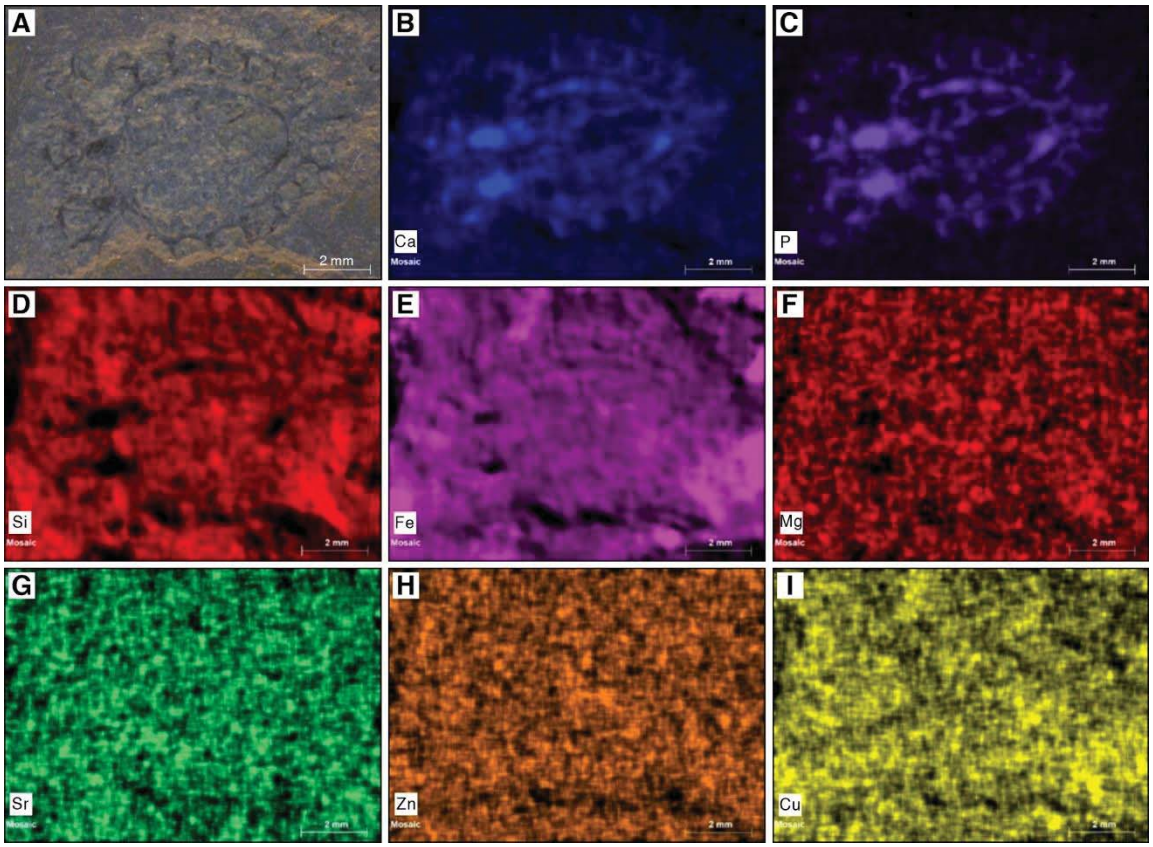


**Fig. S14. µXRF elemental maps for the Cyclida specimen from Xiaba section, showing calcium phosphate preservation.**

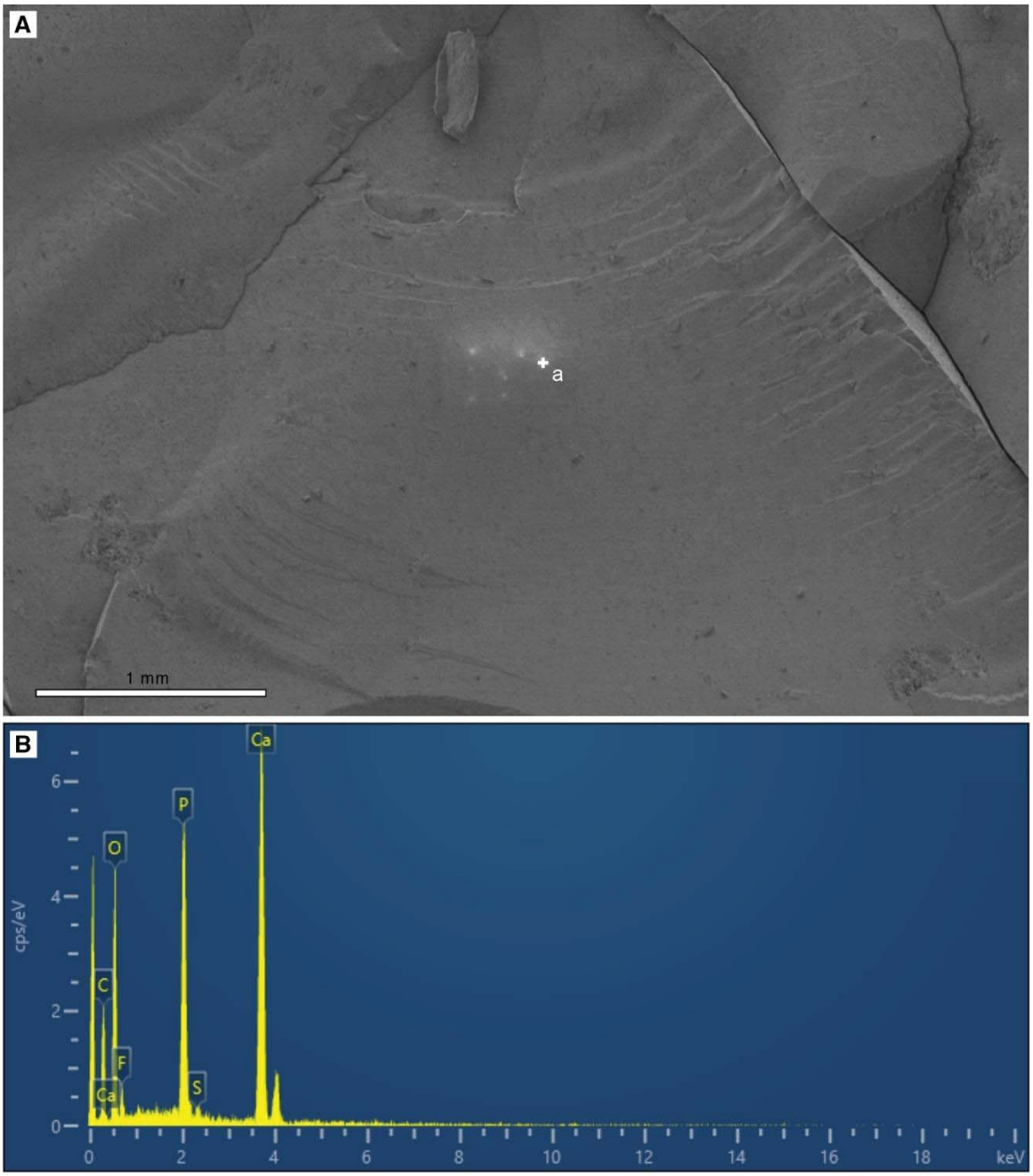


**Fig. S15. SEM photograph and EDS analysis of a coprolite specimen from sample GJ-152B, Gujiao. (A)** SEM photograph, target point for EDS analysis indicated by **a**. **(B)** EDS analysis for target point **a** indicates that the coprolite is preserved in calcium phosphate.

5

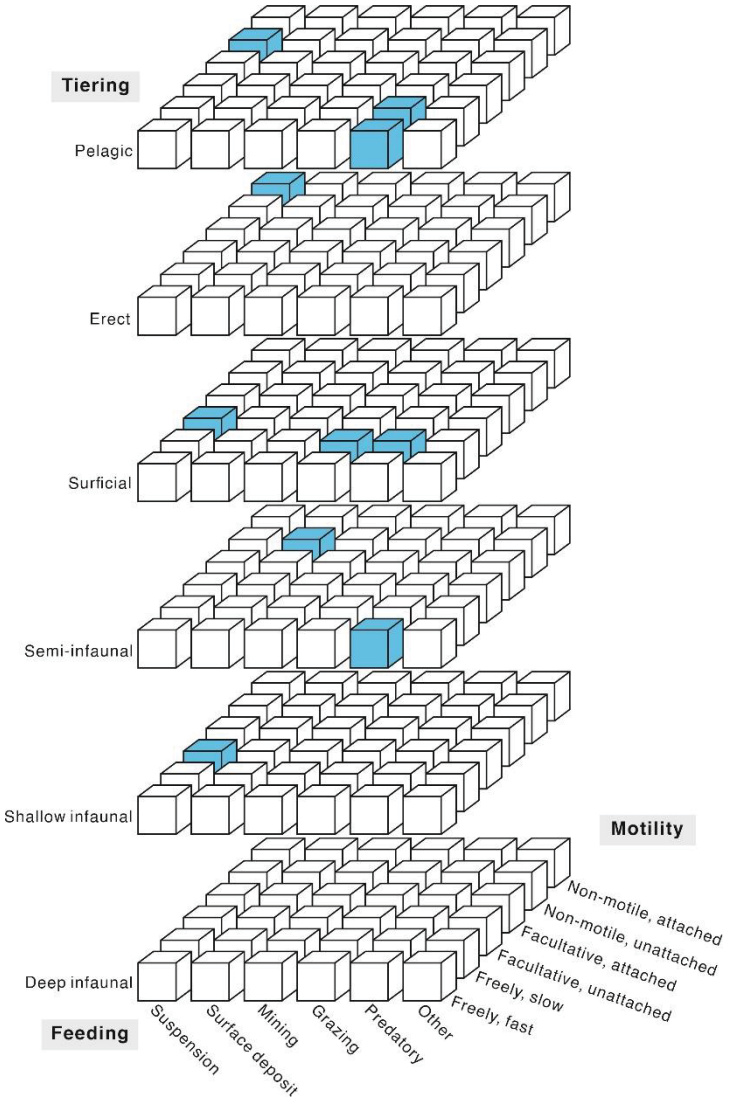


**Fig. S16. Marine community ecological categories for tiering, feeding mechanism, and motility level.** The blue cubes represent categories occupied by the Guiyang Biota.

| Sample | height (cm) | $\delta^{13}C$ | $\delta^{18}O$ |
|---|---|---|---|
| GJ-240 | 5063 | 2.16 | -6.18 |
| GJ-228 | 4729 | 3.23 | -6.20 |
| GJ-212 | 4226 | 4.21 | -6.06 |
| GJ-199 | 3943 | 4.62 | -6.16 |
| GJ-192 | 3767 | 4.90 | -5.66 |
| GJ-181 | 3491 | 4.35 | -6.47 |
| GJ-175 | 3338 | 3.47 | -5.27 |
| GJ-161 | 3043 | -1.76 | -5.87 |
| GJ-151 | 2741 | -6.44 | -5.64 |
| GJ-149 | 2702 | -6.69 | -5.52 |
| GJ-146 | 2596 | -0.71 | -6.71 |
| GJ-140 | 2426 | 1.36 | -6.68 |
| GJ-130 | 2219 | -1.89 | -6.58 |
| GJ-122 | 2026 | 0.67 | -7.21 |
| GJ-110 | 1641 | -3.01 | -5.87 |
| GJ-100 | 1371 | 0.59 | -6.59 |
| GJ-90 | 1193 | 0.36 | -6.28 |
| GJ-80 | 1039 | 0.96 | 13.08 |
| GJ-70 | 915 | 0.13 | -5.95 |
| GJ-50 | 645 | 1.12 | -5.90 |
| GJ-40 | 499 | 0.33 | -6.12 |
| GJ-31 | 389 | 0.80 | -6.49 |
| GJ-22 | 260 | 0.57 | -5.51 |
| GJ-11 | 153 | -0.23 | -5.82 |
| GJ-8 | 137 | 0.69 | -4.01 |
| GJ-h | 91 | -0.70 | -3.83 |

**Table S1. Carbon isotope measurements of the Daye Formation at the Gujiao section.**

The height of the Permian/Triassic boundary in Gujiao section is marked as 0 cm.

| | Composition | | | | Isotopic Ratios | | | | | | | | Dates (Ma) | | | | | | | | |
|---|---|---|---|---|---|---|---|---|---|---|---|---|---|---|---|---|---|---|---|---|---|
| | | | | | | | | | | | | | | | | | | | 206Pb/ | | |
| | Th/ | Pb* | Pbc | Pb*/ | 206Pb/ | 207Pb/ | | 207Pb/ | | 206Pb/ | | Corr. | 207Pb/ | ±2σ | 207Pb/ | ±2σ | 206Pb/ | ±2σ | 238U | ±2σ | |
| Fraction | U a | (pg) b | (pg) c | Pbc d | 204Pb e | 206Pb f | ±2σ % | 235U f | ±2σ % | 238U f | ±2σ % | coef. | 206Pb g | abs | 235U g | abs | 238U g | abs | <Th> h | abs | % disc i |
| | | | | | | | | | | | | | | | | | | | | | |
| Sample GJ-ASH-134 | | | | | | | | | | | | | | | | | | | | | |
| GJ134_z2 | 0.55 | 25.3 | 1.34 | 18.97 | 1146 | 0.0512 | 0.57 | 0.28 | 0.6 | 0.039678 | 0.059 | 0.565 | 249 | 13 | 250.6 | 1.3 | 250.83 | 0.15 | 250.92 | 0.15 | -0.9 |
| GJ134_z4 | 0.58 | 17.4 | 1.31 | 13.28 | 802 | 0.0511 | 0.82 | 0.2795 | 0.9 | 0.039684 | 0.1 | 0.813 | 244 | 19 | 250.3 | 2 | 250.87 | 0.25 | 250.96 | 0.25 | -2.62 |
| GJ134_z3 | 0.58 | 12 | 0.82 | 14.65 | 883 | 0.05131 | 0.8 | 0.281 | 0.85 | 0.039742 | 0.071 | 0.714 | 254 | 18 | 251.5 | 1.9 | 251.24 | 0.18 | 251.32 | 0.18 | 0.96 |
| GJ134_z1 | 0.85 | 7.07 | 0.89 | 7.91 | 455 | 0.05122 | 1.6 | 0.2809 | 1.7 | 0.039788 | 0.12 | 0.731 | 250 | 36 | 251.3 | 3.7 | 251.52 | 0.29 | 251.6 | 0.29 | -0.72 |
| | | | | | | | | | | | | | | | | | | | | | |
| Sample GJ-ASH-157 | | | | | | | | | | | | | | | | | | | | | |
| GJ157_z3_1 | 0.43 | 17.8 | 0.3 | 59.96 | 3560 | 0.051309 | 0.14 | 0.28039 | 0.16 | 0.039652 | 0.034 | 0.617 | 253.7 | 3.2 | 250.97 | 0.35 | 250.674 | 0.084 | 250.766 | 0.084 | 1.2 |
| GJ157_z3_2 | 0.43 | 17.8 | 0.29 | 60.33 | 3582 | 0.05131 | 0.14 | 0.28042 | 0.17 | 0.039656 | 0.035 | 0.611 | 253.7 | 3.4 | 250.99 | 0.37 | 250.698 | 0.085 | 250.79 | 0.085 | 1.2 |
| GJ157_z4 | 0.49 | 8.87 | 0.26 | 34.15 | 2003 | 0.05135 | 0.22 | 0.28093 | 0.24 | 0.0397 | 0.034 | 0.522 | 255.3 | 5.1 | 251.39 | 0.53 | 250.971 | 0.084 | 251.061 | 0.084 | 1.71 |
| GJ157_z5 | 0.42 | 13.4 | 0.27 | 48.70 | 2907 | 0.051263 | 0.17 | 0.28061 | 0.18 | 0.039717 | 0.03 | 0.427 | 251.7 | 4 | 251.14 | 0.41 | 251.082 | 0.075 | 251.174 | 0.075 | 0.23 |
| GJ157_z2 | 0.47 | 6.48 | 0.31 | 20.74 | 1232 | 0.05123 | 0.35 | 0.2807 | 0.39 | 0.03976 | 0.054 | 0.675 | 250.2 | 8.1 | 251.24 | 0.86 | 251.35 | 0.13 | 251.44 | 0.13 | -0.45 |
| GJ157_z1 | 0.52 | 6.91 | 0.32 | 21.93 | 1285 | 0.05128 | 0.36 | 0.2814 | 0.41 | 0.039816 | 0.076 | 0.595 | 252.4 | 8.4 | 251.76 | 0.9 | 251.69 | 0.19 | 251.78 | 0.19 | 0.29 |

**Table S2. Single-grain zircon U-Pb dates and isotopic data.**

| Phylum | Class | Order | Taxa |
|---|---|---|---|
| Chordata | Osteichthyes | Coelacanthiformes | Coelacanthiformes indet. A<br>Coelacanthiformes indet. B |
| | | Acipenseriformes | *Errolichthys* sp. |
| | | Palaeonisciformes | Palaeonisciformes indet. |
| | | Perleidiformes | *Teffichthys elegans* |
| | | Parasemionotiformes | *Watsonulus* sp. |
| | | Polzbergiiformes | Polzbergiiformes indet. |
| | | Ptycholepiformes | *Boresomus* sp. |
| | | / | Actinopterygii indet. A |
| | | / | Actinopterygii indet. B |
| | | / | Actinopterygii indet. C |
| | | / | Actinopterygii indet. D |
| | | / | Actinopterygii indet. E |
| | Chondrichthyes | Hybodontiformes | Hybodontiformes indet. |
| | Conodonta | Ozarkodinida | *Novispathodus posterolongatus*<br>*Neospathodus cristagalli*<br>*Neospathodus dieneri* |
| Mollusca | Bivalvia | Pterioida | *Eumorphotis hinnitidae*<br>*Eumorphotis* sp.<br>*Claraia* sp.<br>*Scythentolium* sp. |
| | | Mytilida | *Modiolus* sp. |
| | Cephalopoda | Ceratitida | *Pseudosageceras* sp.<br>*Radioceras* sp.<br>Ammonoid indet. |
| | Gastropoda | / | unidentified gastropod |
| Arthropoda | Malacostraca | Decapoda | Litogastridae indet.<br>*Anisaeger* sp.<br>Aegeridae indet. |
| | Multicrustacea | Cyclida | cf. *Yunnanocyclus* |
| | Ostracoda | ? | unidentified ostracod |
| Porifera | ? | ? | sponge spicule |
| Radiolaria | Latentifistularia | Latentifistulidae | *Latentifistula* sp. |
| Foraminifera | Tubothalamea | Miliolida | *Postcladella kalhori*<br>*Planiinvoluta* sp. |
| | Nodosariata | Lagenida | *Rectostipulina* sp.<br>*Tezaquina* sp.<br>*Rectostipulina quadrata*<br>*Nodosinelloides* sp.<br>*Nodosinelloides aequiampla* |

**Table S3. Taxonomic composition of the Guiyang Biota.**

| Groups | Guiyang | Paris | Chaohu | Luoping | Xingyi | Guanling |
|---|---|---|---|---|---|---|
| Reptilia | 0 | 0 | 6 | 8 | 13 | 13 |
| Osteichthyes | 13 | 2 | 2 | 28 | 17 | 6 |
| Chondrychtyes | 1 | 2 | 0 | 2 | 0 | 0 |
| Conodonta | 3 | 1 | 7 | 3 | 0 | 4 |
| Cephalopoda | 3 | 4 | 2 | 2 | 3 | 10 |
| Bivalvia | 5 | 15 | 2 | 1 | 1 | 11 |
| Gastropod | 1 | 0 | 0 | 1 | 0 | 0 |
| Ostracoda | 1 | 0 | 0 | 0 | 0 | 0 |
| Brachiopoda | 0 | 3 | 0 | 1 | 0 | 2 |
| Malacostraca | 3 | 6 | 0 | 12 | 1 | 0 |
| Xiphosura | 0 | 1 | 0 | 1 | 0 | 0 |
| Thylacocephala | 0 | 3 | 4 | 0 | 0 | 0 |
| Cyclida | 1 | 0 | 0 | 1 | 0 | 0 |
| Echinoidea | 0 | 0 | 0 | 1 | 0 | 0 |
| Ophiuroidea | 0 | 1 | 0 | 0 | 0 | 0 |
| Crinoidea | 0 | 1 | 0 | 1 | 1 | 3 |
| Holothurians | 0 | 0 | 0 | 0 | 0 | 1 |
| Porifera | 1 | 2 | 0 | 0 | 0 | 0 |
| Radiolarian | 1 | 0 | 0 | 0 | 0 | 0 |
| Chlorophytae | 0 | 4 | 0 | 0 | 0 | 0 |
| Foraminifera | 7 | 0 | 7 | 0 | 0 | 0 |

**Table S4. Species richness of major fossil groups of the studied Triassic biotas.** See Data S1 for detailed taxonomic list.

| Ecological guilds | | | Guiyang | Paris | Chaohu | Luoping | Xingyi | Guanling |
|---|---|---|---|---|---|---|---|---|
| **Tiering** | **Feeding** | **Motility** | | | | | | |
| Pelagic | Predatory | Freely, fast | 20 | 9 | 17 | 43 | 33 | 33 |
| Pelagic | Predatory | Freely, slow | 2 | 2 | 0 | 4 | 0 | 0 |
| Pelagic | Suspension | Non-motile, attached | 1 | 0 | 0 | 0 | 0 | 3 |
| Erect | Other | Non-motile, attached | 0 | 4 | 0 | 0 | 0 | 0 |
| Erect | Suspension | Non-motile, attached | 1 | 4 | 0 | 1 | 1 | 0 |
| Surficial | Predatory | Freely, slow | 1 | 6 | 4 | 6 | 1 | 0 |
| Surficial | Grazing | Freely, slow | 2 | 1 | 0 | 2 | 0 | 0 |
| Surficial | Suspension | Facultative | 4 | 14 | 2 | 1 | 1 | 12 |
| Surficial | Suspension | Non-motile, attached | 0 | 0 | 0 | 0 | 0 | 1 |
| Semi-infaunal | Predatory | Freely, fast | 1 | 2 | 0 | 2 | 0 | 0 |
| Semi-infaunal | Surface deposit | Non-motile, unattached | 7 | 0 | 7 | 0 | 0 | 0 |
| Shallow infaunal | Predatory | Freely, fast | 0 | 0 | 0 | 2 | 0 | 0 |
| Shallow infaunal | Suspension | Facultative | 1 | 3 | 0 | 1 | 0 | 1 |

**Table S5. Species richness of ecological guilds of the studied Triassic biotas.** See Data S1 for detailed list.

| Tube parameter | Values | Mapping parameters | Values |
|---|---|---|---|
| High voltage (KV) | 50 | Width (mm) | 30.611 (612 pixels) |
| Anode current (mA) | 200 | Height (mm) | 23.492 (470 pixels) |
| Filter | Empty | Pixel size (µm) | 50 |
| Optic | Lens | Total number of pixels | 287 640 |
| Spot Size | 20 | **Acquisition parameters** | **Values** |
| Chamber (mbar) | Air 20 | Frame count | 1 |
| Anode | Rh | Pixel time (ms/pixel) | 100 |
| **Detector parameters** | **Values** | Measure time (h) | 7.35 |
| Selected detectors | 1 | Overall time (h) | 9 |
| Max. pulse throughput (cps) | 130 000 | Stage speed (µm/s) | 50 |

**Table S6. Operating conditions of Micro-XRF.**